MDPI

Article

Geology, Petrology, and Mineralogy of Hornfels-like Rocks (Beerbachite) in the Early Paleozoic Olkhon Collisional Orogen (West Baikal Area, Russia)

Eugene V. Sklyarov [1,*], Sergei A. Kargopolov [2,3], Andrey V. Lavrenchuk [2,3], Evgenii V. Pushkarev [4] and Dina V. Semenova [2]

1   Institute of the Earth's Crust, Siberian Branch of the Russian Academy of Sciences, 128 Lermontov St., 664033 Irkutsk, Russia
2   V.S. Sobolev Institute of Geology and Mineralogy, Siberian Branch of the Russian Academy of Sciences, 3 Akad. Koptyuga St., 630090 Novosibirsk, Russia; toask@mail.ru (S.A.K.); alavr@igm.nsc.ru (A.V.L.); semenovadina@gmail.com (D.V.S.)
3   Department of Geology and Geophysics, Novosibirsk State University, 2 Pirogov St., 630090 Novosibirsk, Russia
4   A.N. Zavaritsky Institute of Geology and Geochemistry, Uralian Branch of the Russian Academy of Sciences, Akad. Vonsovsky St., 620016 Ekaterinburg, Russia; pushkarev.1958@mail.ru
*   Correspondence: skl@crust.irk.ru; Tel.: +7-914-908-9408

Abstract: Geological, mineralogical, and petrological observations are reported for hornfels-like fine-grained granular mafic rocks in the Early Paleozoic Olkhon collisional orogen (West Baikal area, Russia). The rocks are composed of orthopyroxene, clinopyroxene, amphibole, plagioclase, and ilmenite; some samples also contain olivine, phlogopite, spinel, and titanomagnetite (Opx+Cpx+Amp+Pl+Ilm±Ol±Bt±Spl±Ti-Mag). There are three occurrences of these rocks in the area: a 500 m × 1000 m field in the Shirokaya Valley, another occurrence within the Tazheran Massif (a complex of igneous and metamorphic rocks), and dismembered dikes on the southern margin of the Birkhin gabbro intrusion. The Shirokaya field is located between two 500 Ma intrusions of the Birkhin gabbro; the Tazheran occurrence coexists with syenite, including nepheline syenite, subalkaline gabbro, and marble protrusions; and the dismembered dikes coexist with carbonates and display progressive alteration of dolerite through typical granular varieties. The dikes associated with granite and marble veins mark a part of a large arc-shaped shear zone that traverses the whole intrusive body produced by rotation of a rigid gabbro block during the peak of tectonic deformation at 470–460 Ma. All three occurrences of the hornfels-like rocks lack any evident source of heat that would be responsible for the thermal alteration of the igneous protolith. We hypothesize that the precursor, subvolcanic dolerite, may have undergone autometamorphism maintained by self-generated heat. Mafic magma intruded during high-rate strike–slip faulting, which caused rapid recrystallization of magmatic minerals and produced the observed metamorphic structures. Proceeding from the controversy in the formation mechanisms, with a heat source required for hornfels but lacking from the sampled occurrences of hornfels-like rocks, we suggest identifying the latter as beerbachite, though the term has mostly fallen into disuse. The reason is that the Olkhon rocks we study have a mineralogy, structure, and texture that are perfectly identical to those of beerbachites described in publications from the first half of the 20th century.

Keywords: beerbachite; metamorphism; magmatism; mineralogy; symplectite; Olkhon collisional orogen; West Baikal region

1. Introduction

Some metamorphic rocks discovered within the Olkhon terrane on the western side of central Lake Baikal (southeastern Siberia, Russia) are remarkable for their hornfels-like features, granular textures, and mafic compositions, with a typical mineral assemblage of Opx+Cpx+Amp+Pl+Ilm±Ol±Bt±Spl±Ti-Mag (here and below mineral abbreviations are after [1]). For several reasons discussed in detail below, the rocks cannot be identified

as hornfels, which commonly form under the thermal effect of hot intrusive material on igneous or sedimentary protoliths. On the other hand, the Olkhon hornfels-like granular rocks are perfectly identical in their mineralogy, structure, and texture to the metamorphic rocks described earlier as beerbachite. That is why we suggest this obsolete and abandoned term for the Olkhon rocks we study.

The term beerbachite was coined by C. Chelius [2] in the late 19th century and applied to fine granular two-pyroxene-plagioclase-magnetite (ilmenite) dike rocks with a saccaroid texture found in the Odenwalde gabbro intrusion in Germany. That description by Chelius was included in the book of Rosenbusch [3], a classical treatise that was a bible for many geologists in the first half of the 20th century. The Odenwalde beerbachite [2] was later reinterpreted by Klemm [4] as metamorphic sedimentary inclusions of a mafic composition rather than dikes and by MacGregor [5] as hornfels derived from mafic igneous protoliths. Nevertheless, the interpretation of beerbachite as dike rocks in coarser gabbro remained a predominant view, supported by Bloxam [6], MacGregor [5], Phillips [7], Dixey [8,9], Wells [10], etc. In his overview of published and original data, Phillips [7] suggested distinguishing dike and xenolithic beerbachites and explained the metamorphic structures and textures of dike rocks by thermal alteration during intrusion into already crystallized yet still hot gabbro. In later publications (e.g., [11]), beerbachites from different gabbro bodies worldwide were interpreted either as dikes or as metamorphosed country rock xenoliths. In addition to gabbro, beerbachite occurrences were reported from a sheeted dike–gabbro transition zone in an oceanic crust area [12]. However, the publications where beerbachites would be at least mentioned, if not characterized, have been very limited, and the term itself was rejected as redundant. Beerbachite enclosed in gabbro would be identified well enough as a high-temperature mafic variety of hornfels (pyroxene hornfels facies of contact metamorphism). In this respect, the presence of hornfels rather than ordinary dolerite dikes can be attributed to the recrystallization of dolerite under the thermal effect of the still-hot gabbro. Meanwhile, in addition to the mafic xenoliths and dikes in the gabbro, there are granular mafic metamorphic rocks derived from igneous protoliths by heat from uncertain sources. This is the case of metamorphic rocks in the Olkhon terrane we study.

2. Regional Geological Background

2.1. Olkhon Terrane

The Olkhon composite terrane includes Olkhon Island and the adjacent landmass of the western Lake Baikal shore. It belongs to the Early Paleozoic Baikal collisional belt, delineating the southern periphery of the Siberian craton together with the Sludyanka and Kitoikin terranes (Figure 1). The Olkhon terrane is an intricate collage of 500 Ma and 460 Ma genetically different igneous and metamorphic complexes ([13,14] and references therein). The terrane is composed of two major units (Figure 2): (i) Krestovsky subterrane composed of gabbro (over 50% of total rock volume) and metamorphic rocks (marble and amphibolite) and (ii) a package of tectonic units [14] composed mainly by gneisses with lesser amounts of marble, amphibolite, and quartzite, as well as gabbro and granite intrusions and numerous granitic, pegmatitic, and aplitic veins. The formation of the terrane was interpreted [13] as resulting from successive events of thrusting, doming, and strike–slip faulting, with syntectonic high-temperature metamorphism and intrusions of mafic and granitic magmas. The well-documented rocks produced by the three major tectonic events originated in the Early Paleozoic as a result of microcontinent–island arcs and microcontinent–continent collisions [13]. It was the extensive strike–slip faulting that controlled the general tectonic framework of the terrane, consisting of multiple blocks and shear zones that differ in structure, morphology, and composition.

The history of the Olkhon terrane included at least two events of metamorphism that occurred under different P-T conditions [15]. Granulite facies metamorphism, around 500 Ma [16], was restricted to a narrow zone along the collisional suture between the terrane and the Siberian craton. Other metamorphic rocks of the terrane, from granulite to low

amphibole facies (gneiss, amphibolite, marble, etc.), resulted from the collisional activity of 460–470 Ma [16,17].
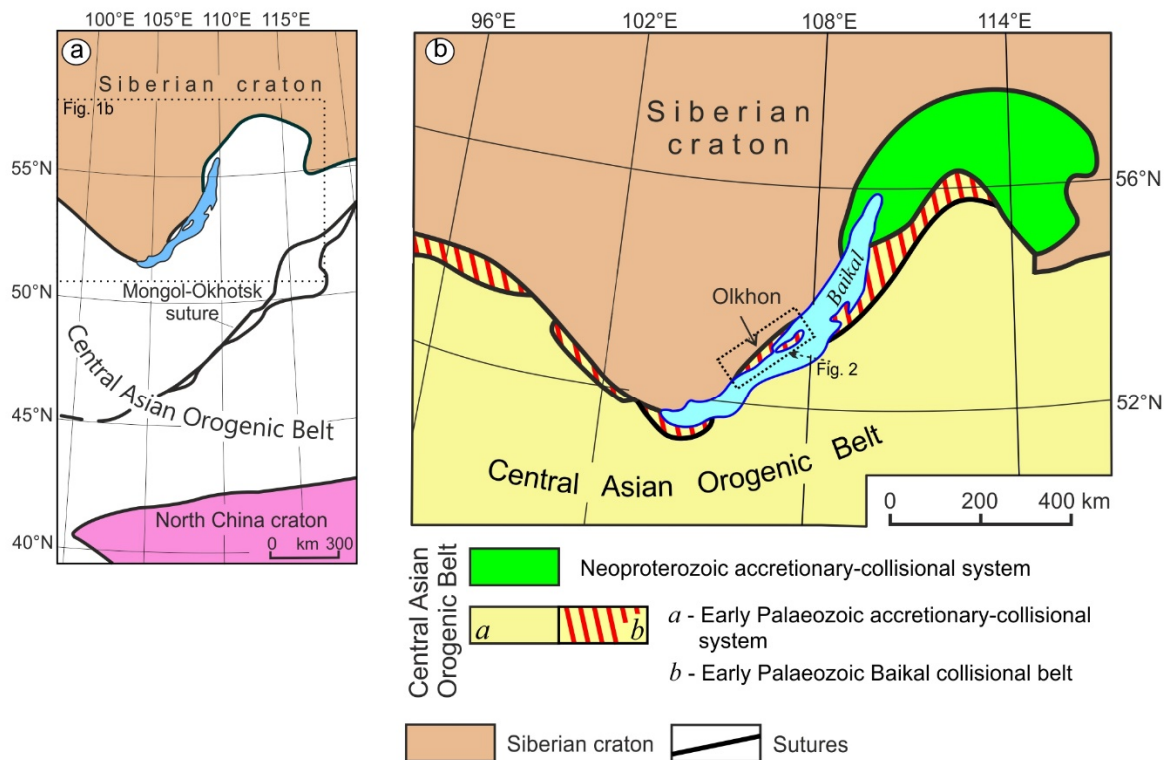

Figure 1. Simplified tectonics of Central Asia (**a**) and metamorphic terranes in the Early Palaeozoic Baikal collisional belt of northern CAOB (**b**), modified after [14].
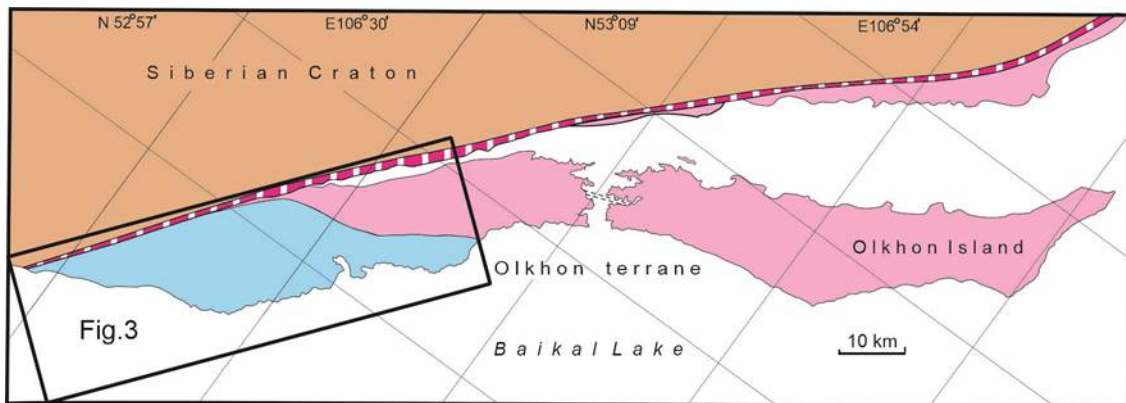

Figure 2. Simplified tectonics of the Olkhon terrane, modified after [14].

2.2. Krestovsky Subterrane

The largest part of the Krestovsky subterrane is occupied by the gabbro of the Birkhin (500 Ma) and Ust'-Krestovsky (460–470 Ma) complexes [18] (Figure 3). The Birkhin volcanoplutonic complex [18,19] consists of gabbro and porphyritic volcanics, often metamorphosed to amphibolite facies, as well as conduit dikes, especially numerous among calcitic marbles in the Baikal coastal cliffs. The origin of the Birkhin complex was previously explained as the magmatism of two phases [20] that produced the Krestovsky, Bora-Elga (phase 1), Buguldeika, Ulan-Nuur (phase 2), and Birkhin (phases 1 and 2) intrusions. The rocks of both phases, including differentiated gabbro and pyroxenite of phase 1 and monzogabbro of phase 2, bear prominent suprasubduction signatures [18]. Most recent data,

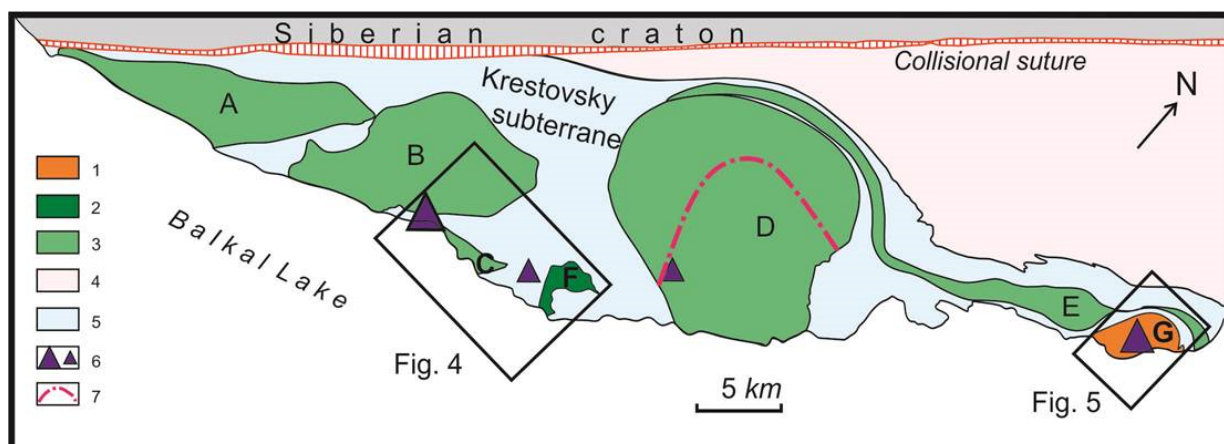however, indicate that the rocks from the two phases represent differentiated ankaramite magma instead [21].

Figure 3. Simplified local geology of the Krestovsky subterrane of the Olkhon terrane: 1 = Tazheran syenite and gabbro, 470–460 Ma (G); 2 = Ust'-Krestovsky intrusion of subalkaline gabbro, 470 Ma (F); 3 = Birkhin gabbro (500 Ma), including Buguldeika (A), Krestovsky (B), Bora-Elga (C), Birkhin (D), and Ulan-Nuur (E) intrusions; 4 = an intricate package of thrust sheets composed mostly of granite and gneiss; 5 = amphibolite and marble of the Krestovsky subterrane; 6 = beerbachite occurrences: fields (large triangles) and altered dikes among gabbro and marble melange (small triangles); 7 = shear zone marked by beerbachite dikes, granite, and marble veins.

The Ust'-Krestovsky complex of gabbro is composed of high-Ti and high-alkaline Ti-fassaite monzogabbro, pyroxenite, and nepheline-Ti augite rocks (phase 1) and phlogopite monzogabbro (phase 2), often altered to amphibolite and gneiss, with moderate Ti contents. The rocks of phase 1 form several small bodies along the sides of the Krestovsky Valley (Figure 4) and are related to high-temperature pyroxene hornfels after the Birkhin porphyrite. Phase 2 rocks occur as part of the Ust'-Krestovsky intrusion within the Krestovsky Valley (Figure 4) and local dikes in marble. They are compositionally similar to subalkaline metagabbro in the Tazheran Massif and composite mafic dikes in northern Olkhon areas [18]. The Ust'-Krestovsky gabbro samples likewise bear suprasubduction signatures but differ from the Birkhin volcanoplutonic rocks in higher contents of Ti and incompatible elements [18].

The Tazheran Massif in the northeastern part of the subterrane is an intricate complex of igneous, metamorphic, and metasomatic rocks (Figure 5) separated from the marble country rocks by a blastomylonite zone of ductile deformation. The igneous rocks are mainly 470 Ma gabbro–dolerite [22] as well as syenite, mostly gneissic, less abundant subalkaline gabbro, commonly gneissic, limited amounts of nepheline syenite, and a few veins of granite and pegmatite. The age of the subalkaline gabbro remains unconstrained within the complex but can be inferred from the age of the compositionally identical Ust'-Krestovsky gabbro dated in other occurrences at 470–460 Ma [18]. Nepheline syenite occurs commonly as linear or intricately shaped veins, from 20 cm to a few meters thick, less often a few tens of meters, with age constraints between 467 Ma and 454 Ma determined by different methods [22]. The granite and pegmatite veins, the youngest igneous bodies in the complex, are limited to a few sites and vary in thickness from 1 m to 10 m. The Tazheran metamorphic rocks are mainly brucite or dolomite-bearing calcite marbles, which were previously interpreted as xenoliths in igneous rocks. On the other hand, they differ from mantle carbonatite in mineralogy and chemistry. Alternatively, a wealth of geological evidence rather suggests an origin by injection nearly synchronously with subalkaline gabbro and nepheline syenite [22]. They may represent melt batches produced by melting sedimentary carbonates in the lower crust and then ascending to emplace at shallower

depths [22]. Diverse, mainly high-temperature metasomatic rocks are found among the Tazheran carbonates.
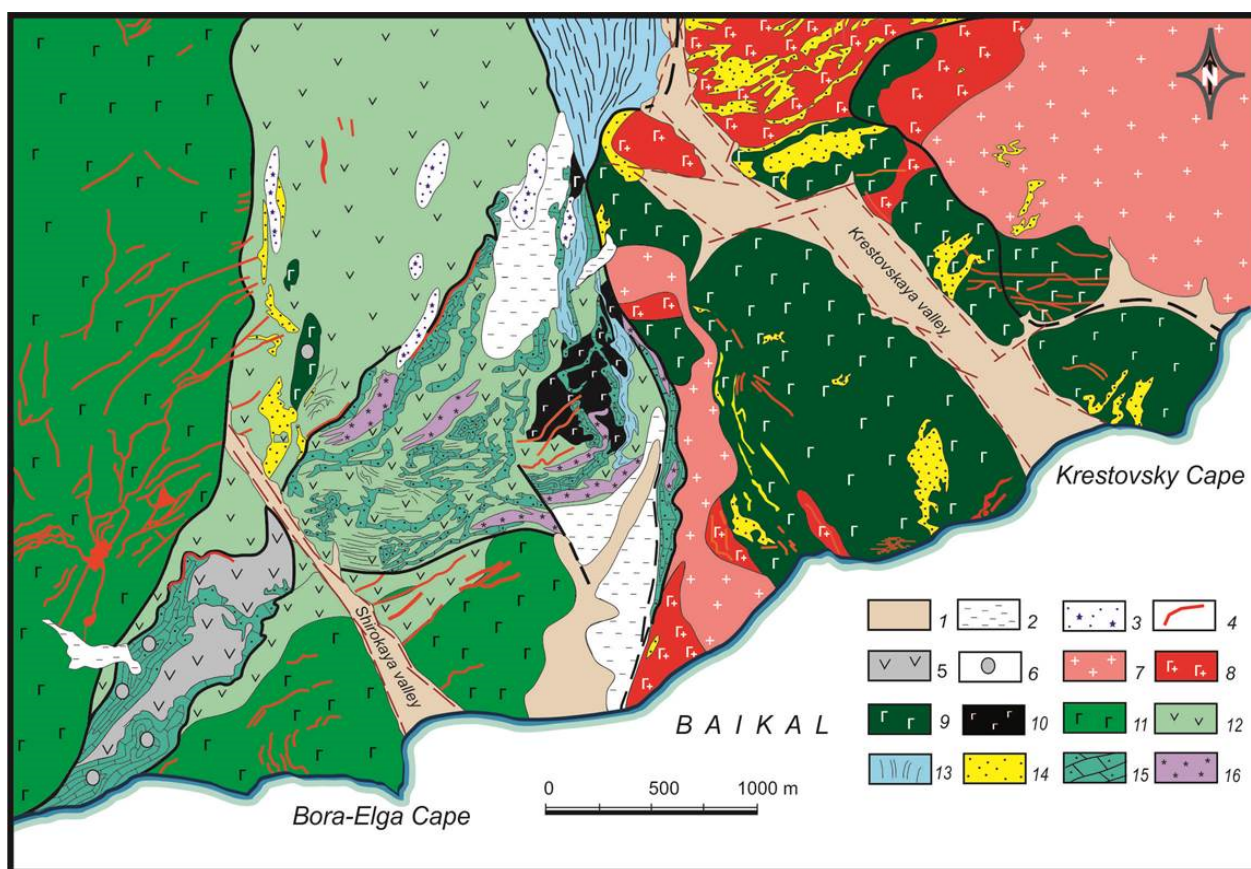

Figure 4. Geological map of the southwestern Krestovsky subterrane: 1 = quaternary alluvium; 2 = quaternary lacustrine–marsh deposits; 3 = quaternary geyserite; 4 = granite veins; 5 = beerbachite, 470 Ma; 6 = small blocks of beerbachite; 7 = Khaidai complex of granite and granodiorite; 8–10 = Ust'-Krestovsky complex of gabbro and granite (485–470 Ma): mingling gabbro, leucogabbro, and syenite (8), monzogabbro, leucomonzogabbro, and quartz-bearing syenite in phase 2 (9), and hybride gabbro in phase 1 (10); 11 = Birkhin gabbro (500 Ma): olivine gabbro, monzogabbro, and monzogabbronorite; 12 = Tsagan–Zaba complex of metaporphyrite and amphibolite after porphyrite (500 Ma); 13 = diopside–quartz–calcite rocks; 14 = injection marble; 15 = marble melange; 16 = quartzite.

Carbonate rocks occupy a large part of the Krestovsky subterrane and are either calcitic or dolomitic varieties. The predominant calcitic marble occurs as elongated bodies in a large field in the central part of the subterrane. Dolomitic and dolomite–calcitic marbles associated with silicic rocks (quartzite, diopside–dolomite–calcite, tremolite–calcite, and quartz–diopside varieties) form an S-shaped band in the southwestern part of the terrane and grade westward into exposures of marble melange. Marble melange is also widespread in the south of the terrane, where it encloses blocks and fragments of silicate rocks ranging from a few mm to tens of meters in size.

The rocks of the Krestovsky subterrane are of low amphibolite metamorphic facies formed mainly at 500–600 °C [15], except for rocks at two sites where the crystallization temperature of minerals reached 800–900 °C. One site is associated with the interaction of phase 1 Ust'-Krestovsky gabbro with the Birkhin metavolcanics (see above), while the origin of the other site in the west remains poorly understood. The idea that the thermal high at the second site would be likewise related to the Birkhin gabbro [23] is inconsistent

with the presence of wide amphibolite zones between the gabbro and the high-temperature metamorphic rocks.
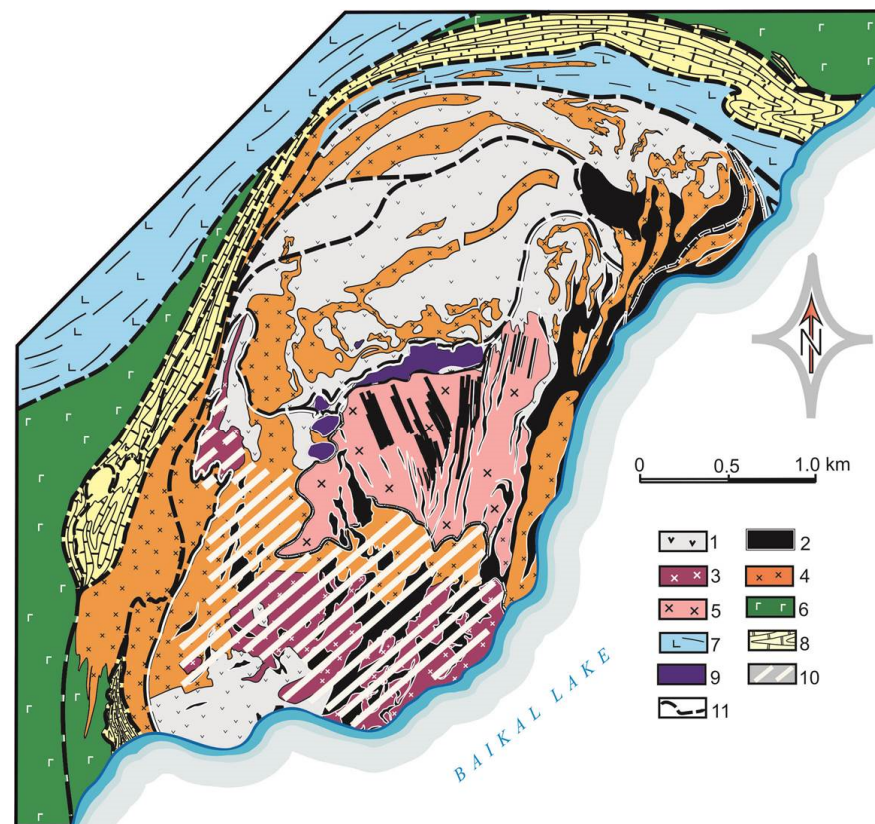

Figure 5. Simplified geology of the Tazheran Massif, modified after [19]: 1–5 = Tazheran complex, 460–470 Ma: beerbachite after tholeiitic dolerite and gabbro (1), subalkaline gabbro and microgabbro (2), nepheline syenite (3), foliated (4), and massive (5) syenites; 6–8 = country rocks: metamorphosed gabbro, monzogabbro, monzonite, and syenite of the Birkhin complex, 500 Ma (6), silicate–carbonate gneiss (7), and calcitic marble (8); 9–10 = fields of occurrences of alkaline (9) and magnesian (10) metasomatic rocks; 11 = synmetamorphic ductile detachment.

Many metasomatic rocks in the Krestovsky subterrane occur along the contacts between different lithologies (e.g., amphibolite and marble) or within shear zones of the Birkhin complex rather than in association with granites or other intrusive rocks. Metasomatism mostly developed at moderate temperatures (garnet–epidote–amphibole–pyroxene, zoisite–amphibole–pyroxene, and other compositions), though high-temperature varieties with melilite, kilchoanite, tilleyite, and other minerals are present as well [24,25]. Judging by their occurrence, the origin of moderate-temperature metasomatic rocks was due to tectonic deformation and syntectonic metamorphism.

3. Beerbachite Geology

Beerbachite rocks are widespread in the southwestern (Shirokaya Valley) and northeastern (Tazheran Massif) parts of the Krestovsky subterrane (Figure 3). The Shirokaya beerbachite appears as 500 m-wide exposures in a long and wide field between the Krestovsky and Bora-Elga gabbro intrusions (Figure 4), flanked by marble melange exposures in the northwest and southeast. The beerbachite and marble melange fields are separated from the gabbro of the Birkhin complex by amphibolite in low amphibolite facies. In addition to the main, thick beerbachite body, there are a few other occurrences: 2–3 m to ~20 m fragments in marble melange; a 30 m × 8 m body within a small intrusion of the Birkhin gabbro

(Figure 4), with buried gabbro–beerbachite contacts; and dismembered dikes in the Birkhin complex and in the marble melange field at the contact with the Ust'-Krestovsky gabbro.

The Tazheran beerbachite makes up a wide field in the northern part of the complex, intruded by syenite bodies of different thicknesses (Figure 5 [22,26]). Most widely spread varieties show well-pronounced thin melanocratic/leucocratic banding.

Dismembered dikes were mapped in the southern periphery of the Birkhin gabbro, where a narrow ($\leq$ 150 m) zone with abundant more or less strongly altered dolerite, as well as injection marble and calciphyre, is traceable for over 1 km (Figure 6). Dolerite along the contact with marble was locally metasomatized under high or moderate temperatures, with the formation of melilite–wollastonite and garnet–pyroxene assemblages, respectively. The zone of dikes spreads discontinuously till the northern margin of the Birkhin gabbro, in the form of a northward-facing arc marked by exposed marble, metadolerite, granite dikes, and metasomatic rocks (Figure 3). The dikes were formed by the rotation of a rigid gabbro block during strike–slip faulting at 470–460 Ma. Some dike fragments vary from 15 to 250 m in length and 3 to 30 m in thickness.
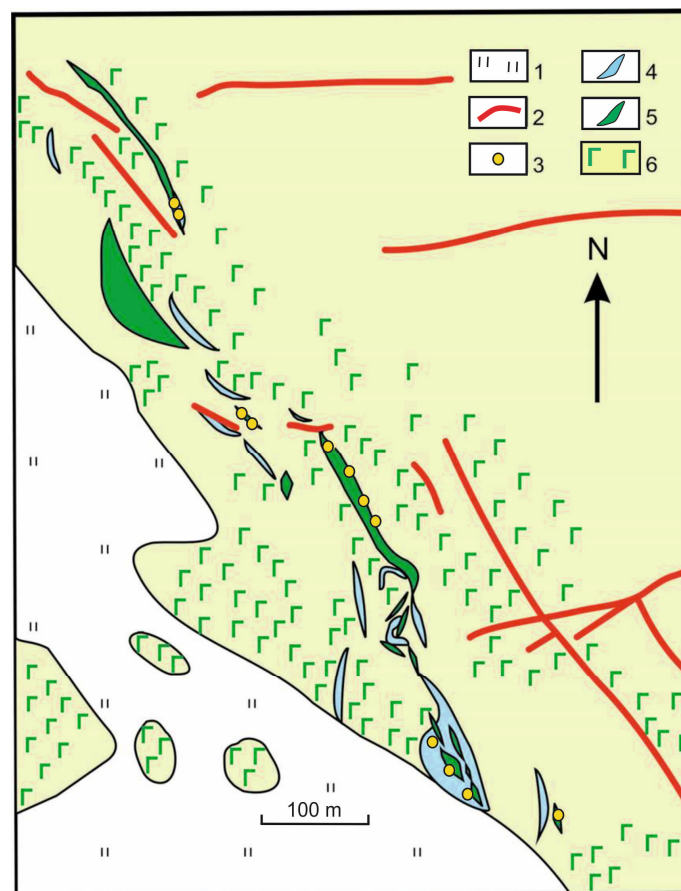

Figure 6. Local geology of the Ozerny site (Birkhin gabbro pluton): (1) lacustrine–alluvial sediments; (2) aplite and granite veins; (3) skarns of garnet–clinopyroxene–wollastonite or more rarely melilite–garnet–pyroxene–wollastonite compositions; (4) carbonate and carbonate–silicate injection rocks; (5) dolerite and beerbachite; (6) Birkhin gabbro (500 Ma).

4. Analytical Methods

Representative beerbachite samples were analyzed for major, trace, and rare-earth elements (REEs). Major elements were analyzed by X-ray fluorescence spectrometry (XRF) on a Bruker AXS *S8 Tiger* spectrometer (Germany) at the Center for Geodynamics and Geochronology (CGG) of the Institute of the Earth's Crust (Irkutsk). Loss on ignition (LOI) was estimated by igniting all samples at 950 °C for 4 h. The ignited sample powders were

fused with lithium borate to prepare beds for the XRF analysis. Calibration curves were constructed using a set of certified reference materials (SRMs): G-2, GSP-2, JG-2, JB-2, BHVO-2, and RGM-1. Accuracy was better than 1% (relative) for most of the major oxides (SiO_2, Al_2O_3, Fe_2O_3, MgO, CaO, K_2O, Na_2O) and 2.5% (relative) for P_2O_5, TiO_2, and MnO. Analytical details are available in [27]. The concentrations of trace elements and rare earth elements were determined by inductively coupled plasma mass spectrometry (ICP-MS) on an Agilent Technologies *Agilent 7500ce* mass spectrometer (USA) at the Limnological Institute (Irkutsk), at the Analytical Center *Ultramikroanaliz*, with sample preparations performed at the CGG. For ICP-MS, the sample powders were fused with lithium borate following the procedure in [28], with adaptations to mafic rocks as described in [27]. The analytical accuracy was better than 5% (relative) for all trace elements and REEs.

The mineralogy of beerbachite samples was analyzed in more than 400 grains of olivine, orthopyroxene, clinopyroxene, amphibole, plagioclase, spinel, and ilmenite in polished thin sections. The analyses were performed at the Analytical Center for Mineralogical, Geochemical, and Isotope Studies of the Geological Institute (Ulan-Ude, Russia) by scanning electron microscopy with energy dispersive X-ray spectroscopy (SEM-EDS) on a LEO 1430VP scanning electron microscope with an Oxford Inca Energy 350 spectrometer. The operation conditions for EDS were: 20 keV beam energy, 0.4 nA beam current, and 50 s spectrum live acquisition time. The results were checked against synthetic compounds and natural minerals: SiO_2 (O, Si), BaF_2 (F, Ba), $NaAlSi_3O_8$ (Na), $MgCaSi_2O_6$ (Mg, Ca), Al_2O_3 (Al), $Ca_2P_2O_7$ (P), $KAlSi_3O_8$ (K), Cr met. (Cr), Mn met. (Mn), and Fe met. (Fe). Matrix correction was performed with the XPP algorithm as part of the built-in Inca Energy software.
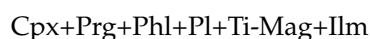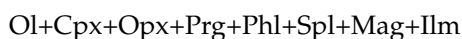
The U-Pb ages of zircons were measured by the laser ablation sector field inductively coupled plasma mass spectrometry (LA–SF–ICP–MS) on a Thermo Fisher Scientific Element XR single-collector high-resolution mass spectrometer coupled to a Teledyne Cetac Analyte Excite excimer laser ablation system equipped with a two-volume HelEx II cell at the Analytical Center for Multi-Elemental and Isotope Research of the Institute of Geology and Mineralogy (Novosibirsk). The ICP–MS was optimized using continuous ablation of an NIST SRM 612 reference glass to provide maximum sensitivity while maintaining low oxide formation $^{248}ThO+/^{232}Th+$ ratios (<1.5%). All measurements were conducted by electrostatic scanning (E-scan) at masses ^{202}Hg, $^{204}(Pb + Hg)$, ^{206}Pb, ^{207}Pb, ^{208}Pb, ^{232}Th, and ^{238}U. The signals were detected in the counting mode for all isotopes except for ^{238}U and ^{232}Th, for which the triple mode was applied. The laser beam diameter was 35 μm, the pulse repetition rate was 5 Hz, and the laser radiation energy density was 4 J/cm^2. Each analysis included 25 s of background measurement followed by 30 s of ablation. Data reduction was carried out with the Glitter software [29]. ^{235}U was calculated from ^{238}U based on the ratio $^{238}U/^{235}U = 137.818$ [30]. Data were corrected for U-Pb fractionation during laser ablation and for instrumental mass discrimination by standard bracketing with repeated measurements of the Plešovice zircon reference material [31]. Accuracy was monitored using the Temora-2 reference material that yielded a concordia age of 413 ± 4 Ma (2σ, n = 8) (417 Ma nominal age; [32]). The data were not corrected for common lead, but monitoring of the signal for 204 allowed excluding affected data from further calculations. Concordia ages and diagrams were generated in Isoplot [33]. Decay constants were borrowed from Steiger and Jäger [34]. Errors are quoted at the 2σ level in all data.

5. Results

5.1. Beerbachite Mineralogy and Petrography

Beerbachite is a dense dark gray to brownish fine to ultrafine granular rock, often massive (Figure 7a) or with well-pronounced thin banding on weathered surfaces (Figure 7b), and with coarser grain sizes at patches and quasi-parallel zones of recrystallization. Locally,

the rock is more or less strongly migmatized and looks gneissic (Figure 7c). The typical mineral assemblages are:

$$Cpx+Opx+Prg+Phl+Pl+Ti\text{-}Mag+Ilm$$

$$Ol+Cpx+Opx+Prg+Phl+Spl+Mag+Ilm$$

$$Cpx+Prg+Phl+Pl+Ti\text{-}Mag+Ilm$$

$$Opx+Prg+Phl+Pl+Ti\text{-}Mag+Ilm$$

5.1.1. Shirokaya Beerbachite

Beerbachite samples from the Shirokaya Valley are mainly melanocratic, almost free from plagioclase (Figure 8a,b), with MgO as high as 18–25 wt.%. The mineralogy consists of olivine, orthopyroxene, clinopyroxene, amphibole, plagioclase (mostly interstitial), and aluminous or chromian spinel as the main phases, less abundant phlogopite and dolomite, and rare accessory zircon or local pentlandite. Additionally, there are opaque minerals of ilmenite, often intergrown with spinel. All melanocratic minerals occur as round or polygonal short-prismatic grains typical of hornfels. The core-to-rim compositional trends in individual grains of Ol, Cpx, Opx, Pl, and Ilm are poorly pronounced or absent. Only some Cr spinels show a rimward decrease in Cr and Fe.

Olivine percentages range from 30%–40% in high-MgO and low-Al_2O_3 varieties to only 10% or even zero in more aluminous rocks. Mg# of olivine corresponds to the whole-rock composition and ranges from 0.75 to 0.50 (Supplementary Table S1), more often being high. The Shirokaya olivine from mafic–ultramafic beerbachite is similar in Mg# to that from Birkhin ankaramite, ultramafic rocks, and gabbro. The contents of Ca and Ni in olivine were below the SEM-EDS detection limit and remain unknown.

Orthopyroxene occurs as short-prismatic or anhedral grains with irregular boundaries. It has 0.8 to 0.6 Mg# (Supplementary Table S2), 0.5 to 2 wt.% Al_2O_3, and < 1 wt.% CaO, which indicates relatively low crystallization temperatures.

Clinopyroxene forms granular, short-prismatic, or anhedral grains. It has a diopside composition at Mg# from 0.91 to 0.75 (Supplementary Table S3). The composition changes from core to rim toward higher Mg# while Al_2O_3 and TiO_2 decrease and CaO increases (e.g., as in clinopyroxene from sample 1788). These changes correspond to a cooling regressive trend, which is reversed by the crystallization trend toward lower Mg# and higher Al_2O_3 and TiO_2 in clinopyroxene from Birkhin ankaramite (Figure 9). Meanwhile, the compositions of clinopyroxene from beerbachite vary within the field of pyroxene from ankaramite.

Cr spinel-Al spinel occurs as abundant fine subhedral crystals enclosed in olivine and other silicates of the Olkhon beerbachite, spotted by their yellow or greenish-brownish colors. Spinels from both Shirokaya and Tazheran beerbachites are often symplectitic with orthopyroxene, clinopyroxene, and amphibole. The major-element compositions change regularly from earlier to later generations (Supplementary Table S6). Earlier spinel has $Cr/(Cr + Al) = 0.6$–0.4 and $\#Mg = 0.1$–0.4 (Figure 10), with alumina becoming progressively higher rimward. Spinel in symplectites almost lacks Cr, and the $Cr/(Cr + Al)$ ratio decreases to zero. Compared to Cr spinel from genetically different ultramafic rocks, spinel in this beerbachite has the lowest Mg# and even falls beyond the field of metamorphic Cr spinel (Figure 11).

Amphibole has a highly variable major-element chemistry. Most amphiboles correspond to magnesian hornblende and partly to tchermakite (Supplementary Table S4) and are commonly more magnesian than pyroxene from the same rocks, which is evidence of metamorphic origin.

Phlogopite occurs as fine reddish-brownish flakes, limited to a few percent in some beerbachite varieties. It has Mg# as in other melanocratic phases (Supplementary Table S5) and no more than 3.5 wt.% TiO_2.
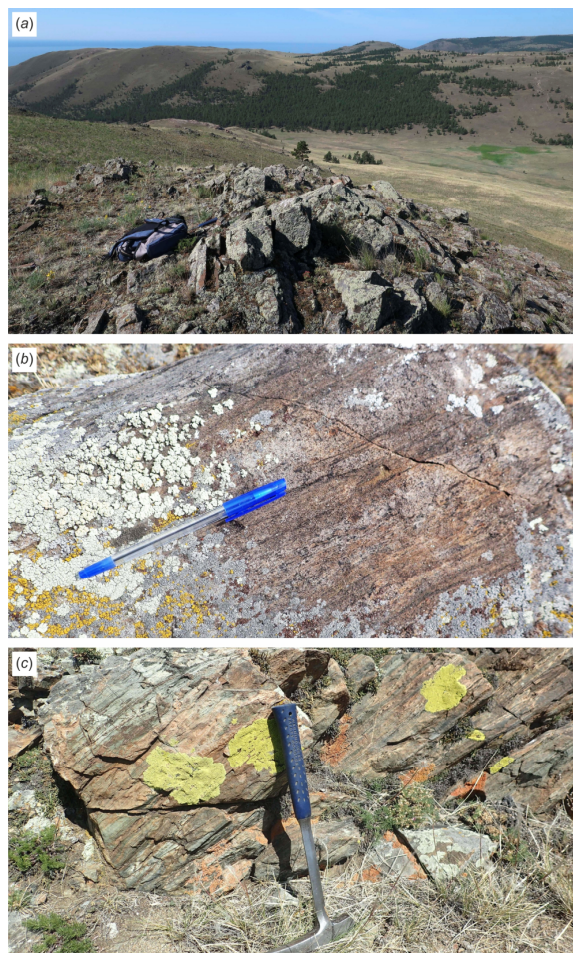

Figure 7. Beerbachite from the Olkhon terrane. (**a**): Outcrop of massive fine beerbachite in the Shirokaya Valley. (**b**): Tazheran beerbachite with thin banding produced by alternating leucocratic and melanocratic layers. (**c**) Migmatized Shirokaya beerbachite.

Plagioclase mainly corresponds to anorthite or, less often, to bytownite (Supplementary Table S7).

In general, minerals in the analyzed beerbachite samples record the conditions of metamorphic recrystallization and the formation of granular textures. Minerals in beerbachite often form sympelctites, especially spinel–orthopyroxene (Figure 12a,b), or less often, spinel–amphibole (Figure 12c) and phlogopite–orthopyroxene (Figure 12d) varieties.

5.1.2. Tazheran Beerbachite

The recrystallization process in the Tazheran beerbachite began with the formation of plagioclase–amphibole or spinel–amphibole symplectites around olivine grains (Figure 13), then led to almost full recrystallization, while the framework plagioclase laths remained (Figure 14a), and finally achieved complete metamorphization. In the consideration below, the samples are conventionally divided into dolerite with preserved magmatic structure (SE315b and SE575a) and metamorphic rocks (SE557a, SE563b, and SE590a).
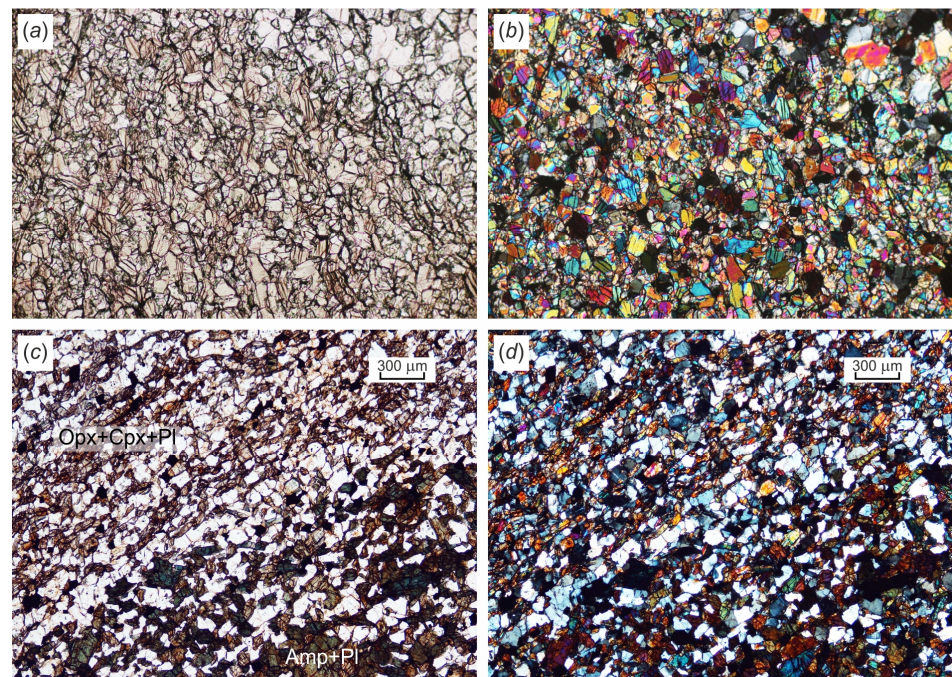
Figure 8. Photomicrographs of Shirokaya beerbachite in plane-polarized (**a**) and cross-polarized (**b**) light. Mineral assemblage: Ol+Opx+Cpx+Amp+Spl+Pl. Panel size: 2.05 × 1.35 mm. (**c,d**): banded leucocratic beerbachite in plane-polarized (**c**) and cross-polarized (**d**) light. Mineral assamblage: Opx+Cpx+Amp+Pl. Banding is produced by alternating leucocratic and melanocratic layers.
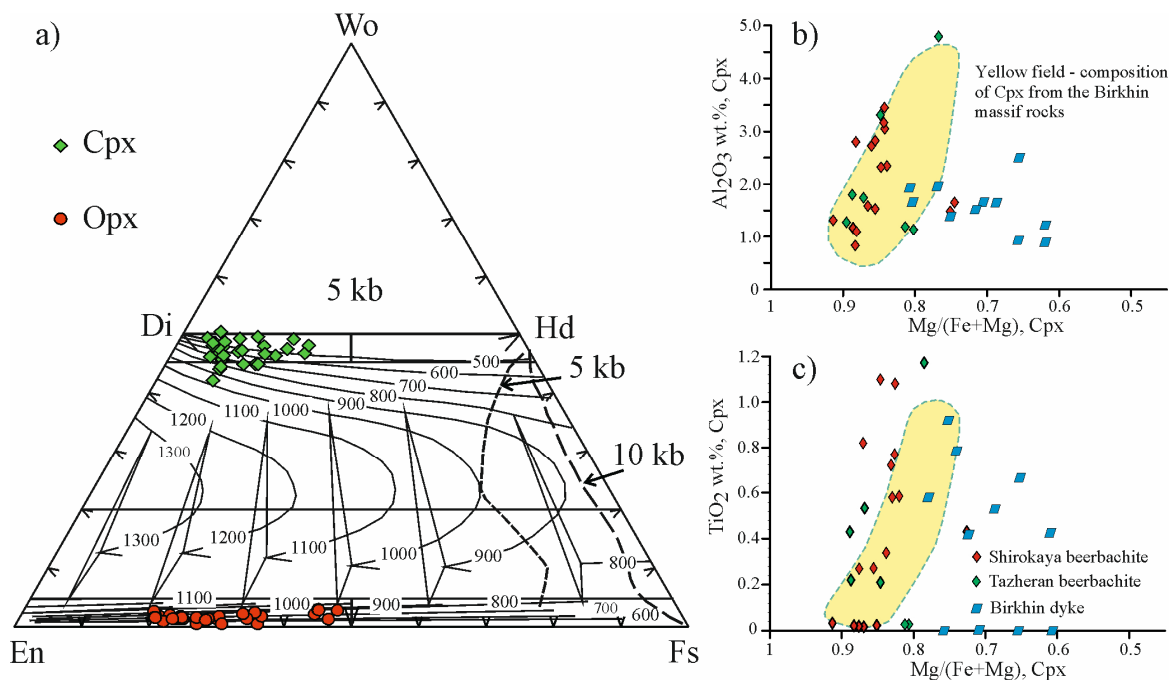

Figure 9. (**a**) Compositions of clinopyroxene (green) and orthopyroxene (red) from high-Mg beerbachite of the Olkhon terrane (undifferentiated) in ternary En-Wo-Fs diagram, after [35]. Thin solid lines are isotherms; dashed lines contour areas beyond pigeonite stability at 5 and 10 kbar. Al_2O_3 (**b**) and TiO_2 (**c**) versus #Mg for clinopyroxenes from high-Mg beerbachite of the Olkhon terrane. Yellow field is composition of clinopyroxene from the Birkhin ankaramite [21].
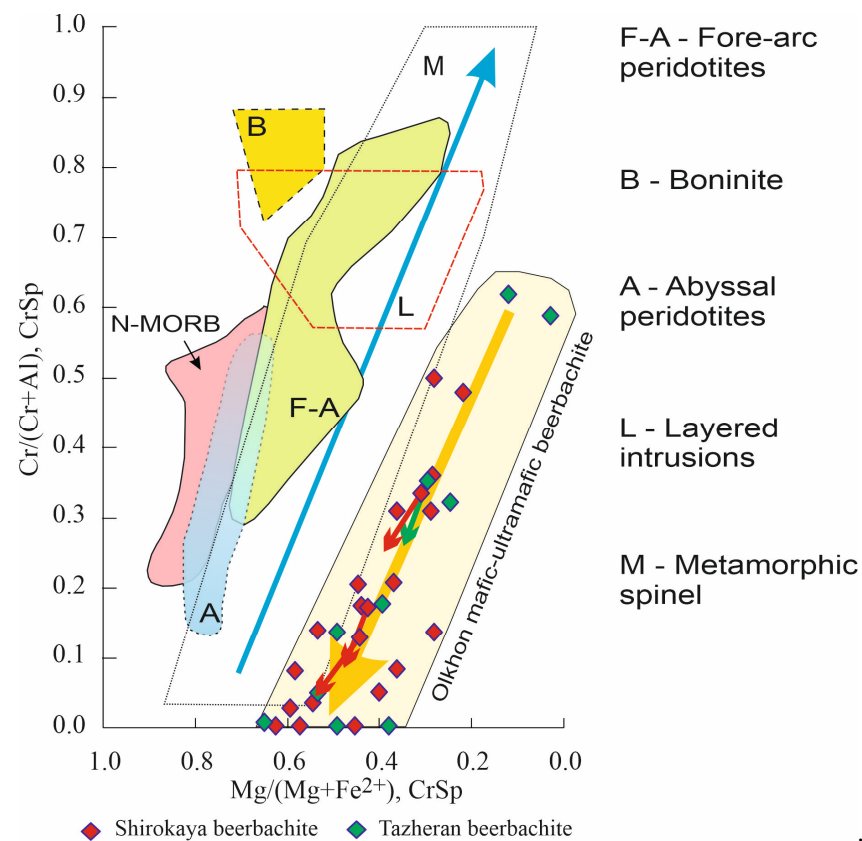
Figure 10. Mg#–Cr# diagram for chromian spinel from high-Mg beerbachite of the Olkhon terrane. Abyssal peridotite, boninite, N-MORB, and layered intrusions are based on [36]; Ural-Alaskan-type intrusions are based on [37]; data for spinel in fore-arc peridotite are based on [38,39]; and the field of metamorphic spinel is based on [40]. Long arrows demonstrate the directions of Cr spinels evolution in ultramafic rocks during metamorphism (blue arrow) and the Olkhon beerbachite Cr spinels during recrystallization (yellow arrow). The changes in composition from the core to the rim of zonal spinels are shown by small red (Shirokaya) and green (Tazheran) arrows.
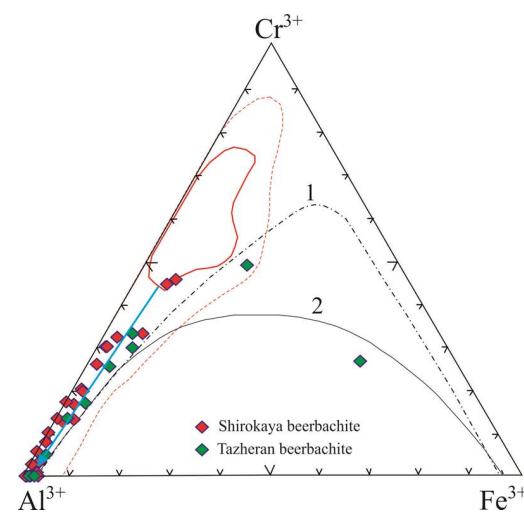

Figure 11. Al-Cr-Fe^{3+} diagram for Cr spinel from high-Mg beerbachite of the Olkhon terrane. 1 = solvus for metamorphic chromite [41], 2 = solvus for Cr spinel of the Stare Ransko complex of layered peridotite and gabbro [42], chromitite excluded [37]. Brown solid and dashed lines refer to 50% and 90% of the data set, respectively. The blue arrow demonstrates the direction of spinel evolution in beerbachite from the earlier Cr spinel to the later Al-rich spinel.
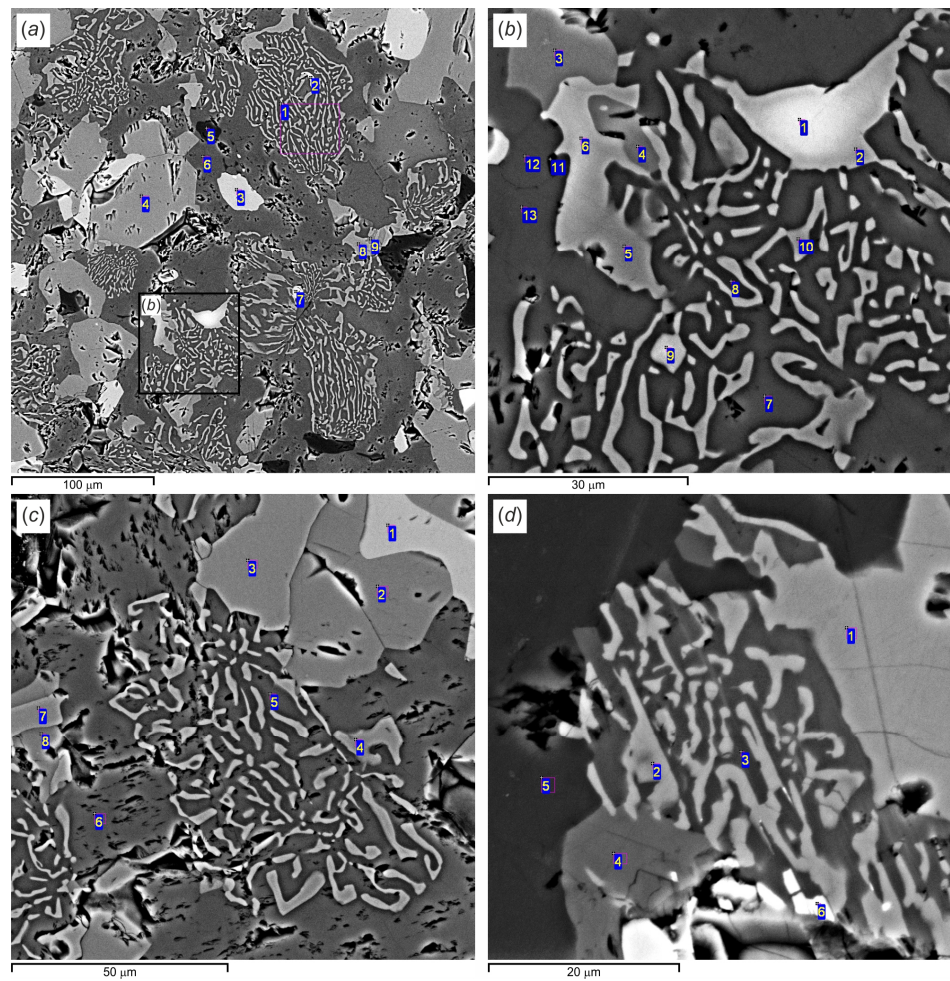
Figure 12. BSE images of symplectites in Shirokaya beerbachite. (**a**): numerous spinel–orthopyroxene symplectites (Sample 1753a): Sympl(1)+Ilm(2)+Ol(3)+Opx(4,9)+Dol(5)+Amp(6)+Apt(7)+Spl(8); (**b**): fragment of panel (**a**): Cr-Spl c(1)+Cr-Spl r (2)+Opx(3,4)+Spl(5)+Cr-Spl(6)+Amp(sympl)(7,8)+Cr-Spl(sympl)(9,10)+Dol(11)+ Amp(12,13); (**c**): amphibole–spinel symplectite (sample 1753a): Ol(1)+Opx(2,8)+Spl(3,4,7)+Amp(5,6); (**d**) phlogopite–orthopyroxene symplectite (sample 1782e): Opx(1)+Mix(2)+Bt(3)+Amp(4)+ Pl(5)+Ol(6). Mix = symplectite. Mineral abbreviations according to [41].
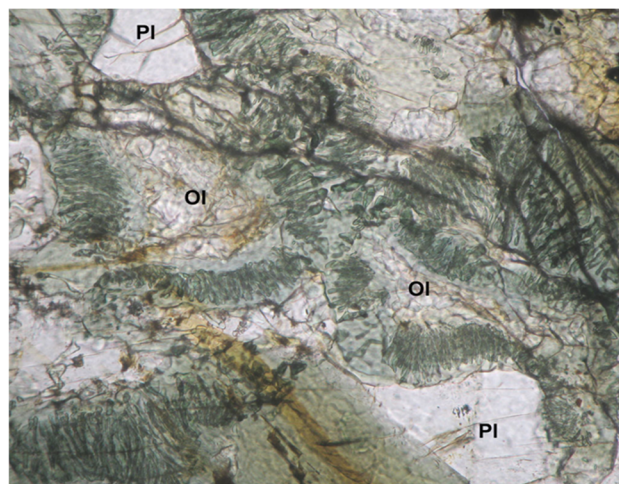

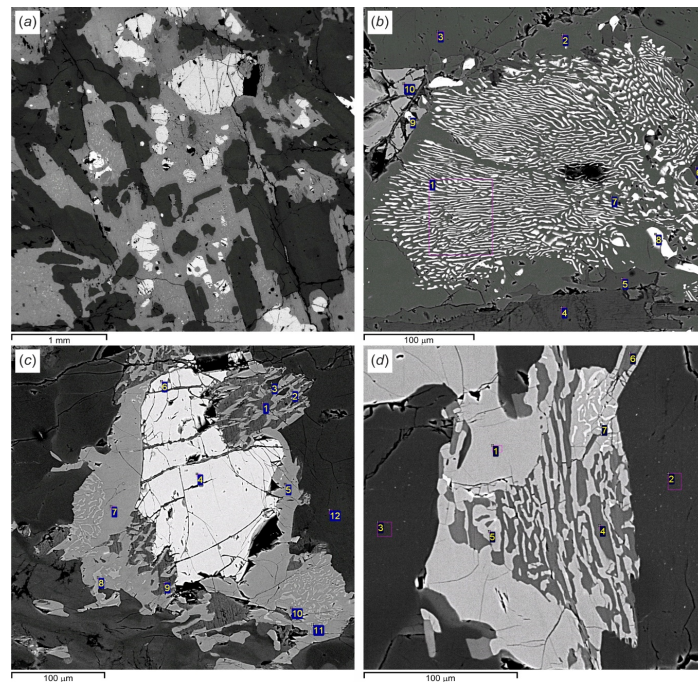**Figure 13.** Olivine–plagioclase coronitic texture (symplectite) in dolerite.

Figure 14. Metadolerite (**a**) and symplectites (**b–d**) in dolerite (sample SE575a): (**a**): ophytic texture in dolerite; plagioclase laths (dark) among mafic minerals. (**b**): orthopyroxene–magnetite–ilmenite symplectite in amphibole. Opx(3,4)+Amph(5,6)+Ilm(1,7)+Mag(2)+Spl(8). (**c**): coarse olivine grain in orthopyroxene coat; orthopyroxene–spinel and orthopyroxene–biotite symplectites along orthopyroxene–plagioclase contacts. Ol(4,6)+Opx(2,5,7,10)+Bt(1,9)+Pl(3)+Spl(8,11). (**d**): orthopyroxene–biotite and orthopyroxene–spinel (right top corner) symplectites. Opx(1,5)+Bt(4,6)+Pl(2,3)+Spl(7).

The most diverse mineralogy in both gabbro and beerbachite corresponds to the assemblage Pl+Hbl+Cpx+Opx+Ol+Bt+Spl, with euhedral grains of olivine, plagioclase, clino- and orthopyroxene, and late magmatic or metamorphic amphibole. The Tazheran mafic rocks show thin banding. The linear structures were apparently formed during both magmatic flow and later metamorphism.

The mineral assemblages of Tazheran and Shirokaya beerbachites are generally similar, but the former differ by signatures of more extensive retrogressive metamorphism and the ensuing loss of olivine and pyroxenes (orthopyroxene or sometimes also clinopyroxene) from the mineral assemblages, while amphibole varied until actinolite and cummingtonite became a predominant phase.

Olivine forms individual grains as well as quite large (up to 1 mm) particles with numerous orthopyroxene, amphibole, plagioclase, and ilmenite inclusions (Figure 15a). Olivine has almost invariable or slightly variable (0.60 to 0.72) Mg# (Supplementary Table S1), higher in olivine from beerbachite than from dolerite (0.70–0.72 vs. 0.60–0.67, respectively).

Orthopyroxene occurs either as individual small grains or numerous symplectites, most often with ilmenite (Figure 15b), spinel (Figure 15c), or phlogopite (Figure 15d) in dolerite. The Mg# ranges are within 0.65–0.79 and totally overlap those for beerbachite and dolerite (Supplementary Table S2). Al_2O_3 contents vary from 1.2 to 3.7 wt.%, and CaO is from 0.25 to 0.82 wt.%. Orthopyroxene is similar to olivine in its mineral chemistry trends. Pyroxenes are quite homogeneous in some samples but show notable variations in others, e.g., either more magnesian (group I) or more ferrous (group II) in sample E575a. See the bimodal Mg# pattern in the histogram of Figure 16.

Clinopyroxene occurs as short-prismatic anhedral grains or, less often, symplectites with spinel (Figure 15e). Major-element chemistry corresponds to diopside, with Mg# ranges of 0.78–0.81 and 0.85–0.89 in dolerite and beerbachite, respectively (Supplementary Table S3), and commonly within 2 wt.% or occasionally 4.84 wt.% Al_2O_3.
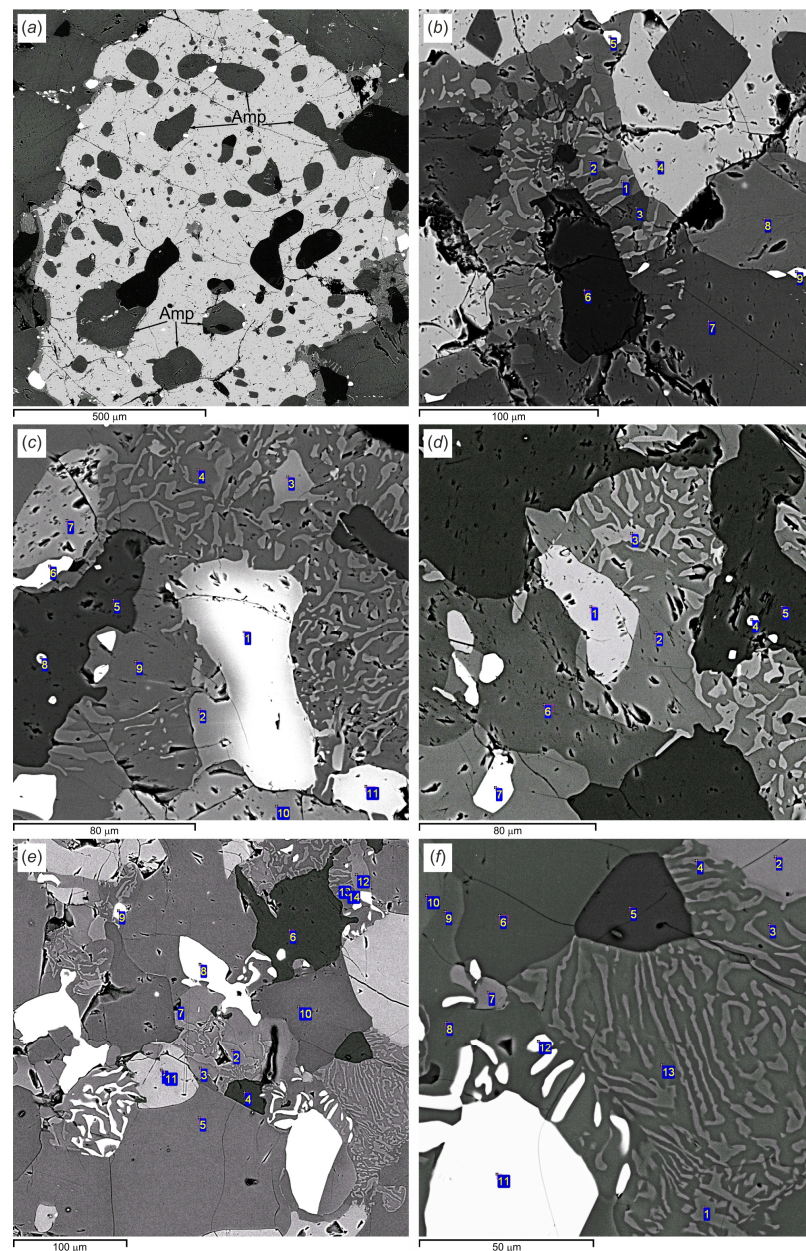
Figure 15. Symplectites in the Tazheran beerbachite. (**a**): coarse grain of poikilitic olivine with amphibole and plagioclase inclusions. (**b**): fragment of panel (**a**); orthopyroxene–spinel symplectite: Spl(1)+Opx(2,8)+Amp(3,7)+Ol(4)+Ilm(5)+Pl(6)+Ti-Mag(9). (**c**): orthopyroxene–spinel symplectite around zoned Cr spinel grain: Cr-Spl(1-3,11)+Cpx(4,9)+ Pl(5)+Ilm(6)+Ol(7,10)+Amp(8). (**d**): orthopyroxene–spinel symplectite around olivine grain: Ol(1)+ Opx(2)+Spl(3)+Cr-Spl(4)+Pl(5)+Amp(6)+Ilm(7). (**e**): Cpx-Spl and Opx-Ilm symplectites: Ol(1,11)+Spl(2,12,13)+Cpx(3)+Pl(4,6)+Opx(5,14)+Dol(7)+Ilm(8)+Ap(9)+Amp(10)'. (**f**): fragment of panel (**e**); clinopyroxene–spinel and orthopyroxene–ilmenite symplectites: Spl(1)+Ol(2,7)+Cpx(3,10,13)+ Pl(5)+Amp(6)+Opx(8,9)+Ilm(11,12).

Most *amphiboles* from beerbachite and dolerite fragments have pargasitic or rarely magnesian hornblende compositions (Supplementary Table S4), with 0.64 to 0.84 Mg# and over 2 wt.% TiO_2 in remnant dolerite and only 1.3 wt.% in beerbachite.

Phlogopite occurs as individual flakes or symplectites with orthopyroxene in dolerite (Figure 14d). Mg# is within 0.71–0.82 (Supplementary Table S5) while TiO_2 varies from

0.19 to 5.82 wt.% due to the coexistence of magmatic and metamorphic phlogopite. The phlogopite grains with the lowest Ti contents have higher Mg#.
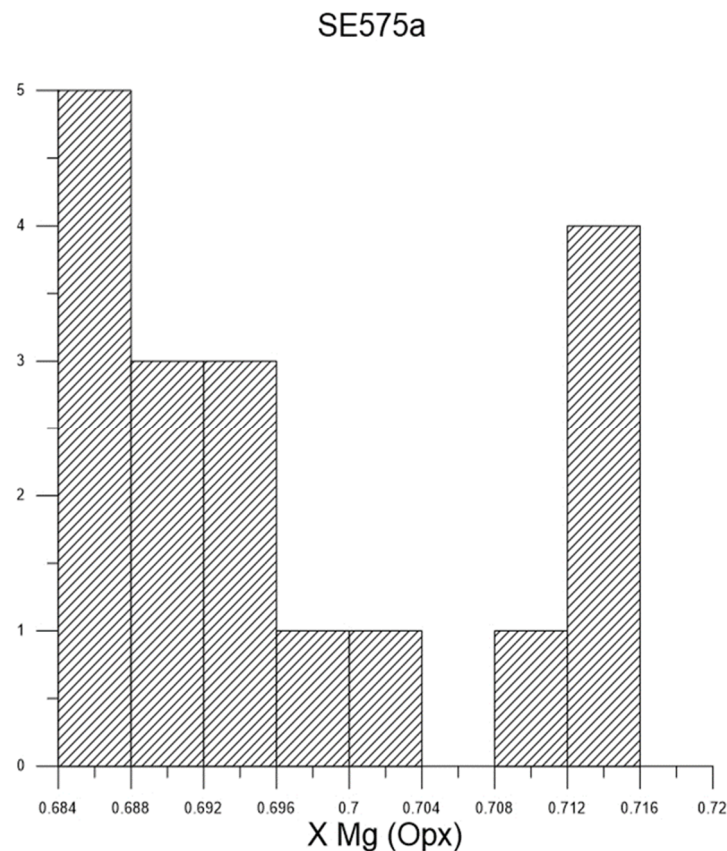

Figure 16. Bimodal distribution of X_{Mg} in orthopyroxene from sample SE575a.

Spinel and *Cr spinel* varieties are present in all analyzed samples and show large element ranges (Supplementary Table S6). All spinel in dolerite is free from Cr (pleonastic composition) and occurs only in symplectites with orthopyroxene, while spinel in almost all beerbachite samples contains 0.6 to 31 wt.% Cr_2O_3. The Cr contents are the highest in relatively large (>100 μm) irregularly shaped zoned grains (Figure 15c) and vary from pleonastic to picotitic compositions in spinel for some samples. Cr_2O_3 decreases toward grain rims and is markedly lower in spinel symplectites with clinopyroxene.

Ilmenite contains maximum MgO concentrations exceeding 4 wt.%, as in the case of Shirokaya beerbachite, while MnO concentrations range from 0.4 to 2.1 wt.% (Supplementary Table S8).

5.1.3. Birkhin Beerbachite

Some mafic igneous bodies at the sampled site consist of weakly altered dolerite, and some others are fully beerbachitic, but most often dolerite and beerbachite coexist within a body. The mineral assemblage is Opx + Cpx + Amp + Bt + Pl + Mag + Ilm ± Spl. The transition from dolerite (Figure 17a,b) to classical beerbachite (Figure 17e,f) is continuous and gradual. Unaltered dolerite sometimes hosts thin veinlets of fassaitic pyroxene. Intermediate varieties bear fine aggregates of orthopyroxene and clinopyroxene instead of interstitial pyroxene, while plagioclase retains an ophitic texture (Figure 17c,d). The rocks most similar to beerbachite in their structure and texture have a saccharoid matrix specked with corroded plagioclase laths.

The beerbachite samples are mesocratic, composed of olivine, orthopyroxene, clinopyroxene, amphibole, biotite, and ilmenite, with rare Cr spinel or Cr magnetite.

Olivine occurs as quasi-isometric (Figure 18a,b) or irregularly shaped elongated grains (Figure 18c,d), quite often rimmed with amphibole or orthopyroxene. The compositions vary from moderately magnesian (#Mg 0.55–0.60), similar to some Shirokaya Valley and Tazheran beerbachite varieties, to ferroan (#Mg 0.39–0.44), absent from other beerbachite occurrences (Supplementary Table S1). However, the mineral chemistry is rather homogeneous within each sampled dike fragment.
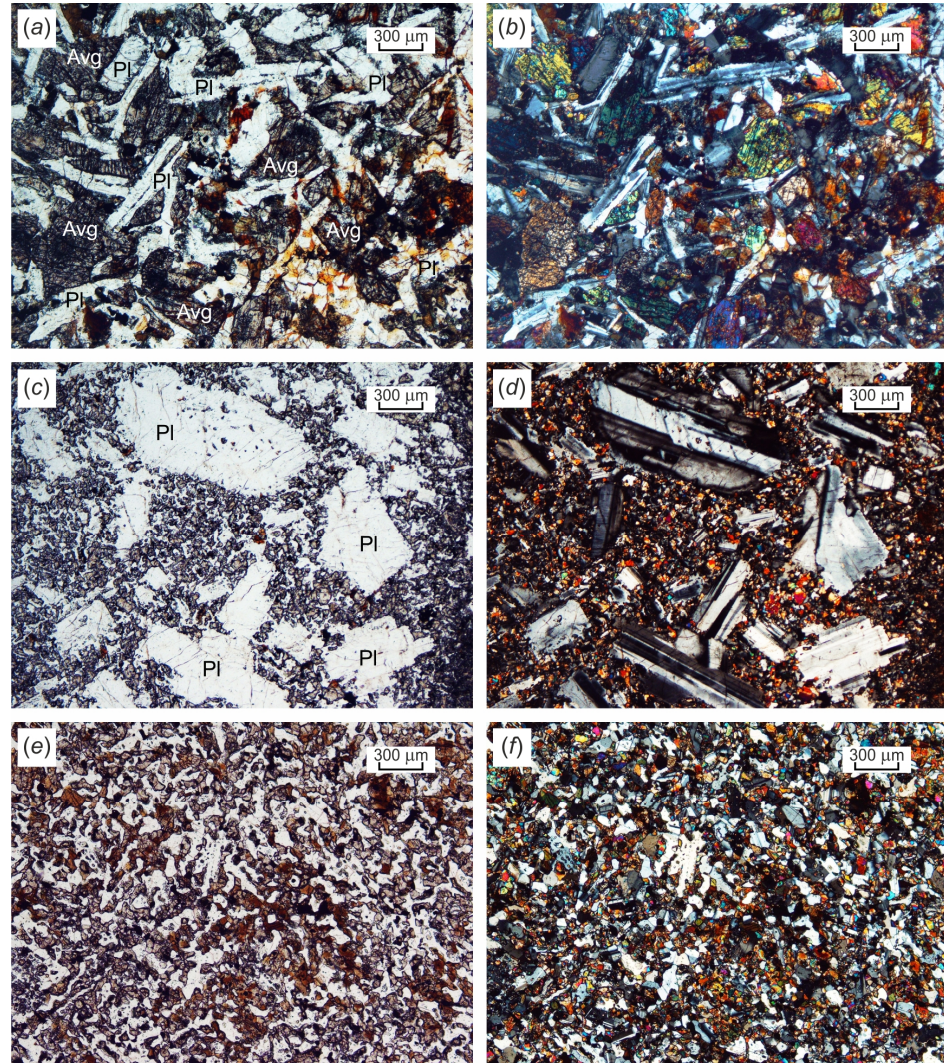

Figure 17. Photomicrographs of beerbachite samples (thin sections). (**a**,**b**): dolerite composed of augite and plagioclase; augite in the rim is partly recrystallized. (**c**,**d**): beerbachite with preserved magmatic structure but with mafic minerals fully recrystallized to an aggregate of fine olivine, orthopyroxene, clinopyroxene, and biotite grains. (**e**,**f**): beerbachite with resorbed plagioclase laths. Melanocratic minerals appear as aggregates of fine olivine, orthopyroxene, clinopyroxene, and biotite grains.

Orthopyroxene appears as elongated, irregularly shaped grains (Figure 18d) or, most often, as rims over olivine or amphibole (Figure 17c), and less often as lamelli in clinopyroxene (Figure 18d). #Mg varies from 0.42 to 0.69 in different dike fragments but has a narrower range of 0.53–0.58 within individual samples. Al_2O_3 ranges from 0.64 to 2.34 wt.% (Supplementary Table S2).

Clinopyroxene, like other melanocratic minerals, forms short-prismatic granular anhedral grains or sometimes encloses orthopyroxene lamelli (Figure 18d) exsolved from primary pyroxene. The #Mg range is from 0.64 to 0.82, as in other mafic minerals; the con-

tent of Al_2O_3 varies from 0.94 to 1.97 wt.%, but locally reaches 8.31 wt.%; TiO_2 is generally from 0 to 2.49 wt.% and may vary from 0.63 to 2.49 wt.% (Supplementary Table S3) even within one sample (e.g., SE01R1).
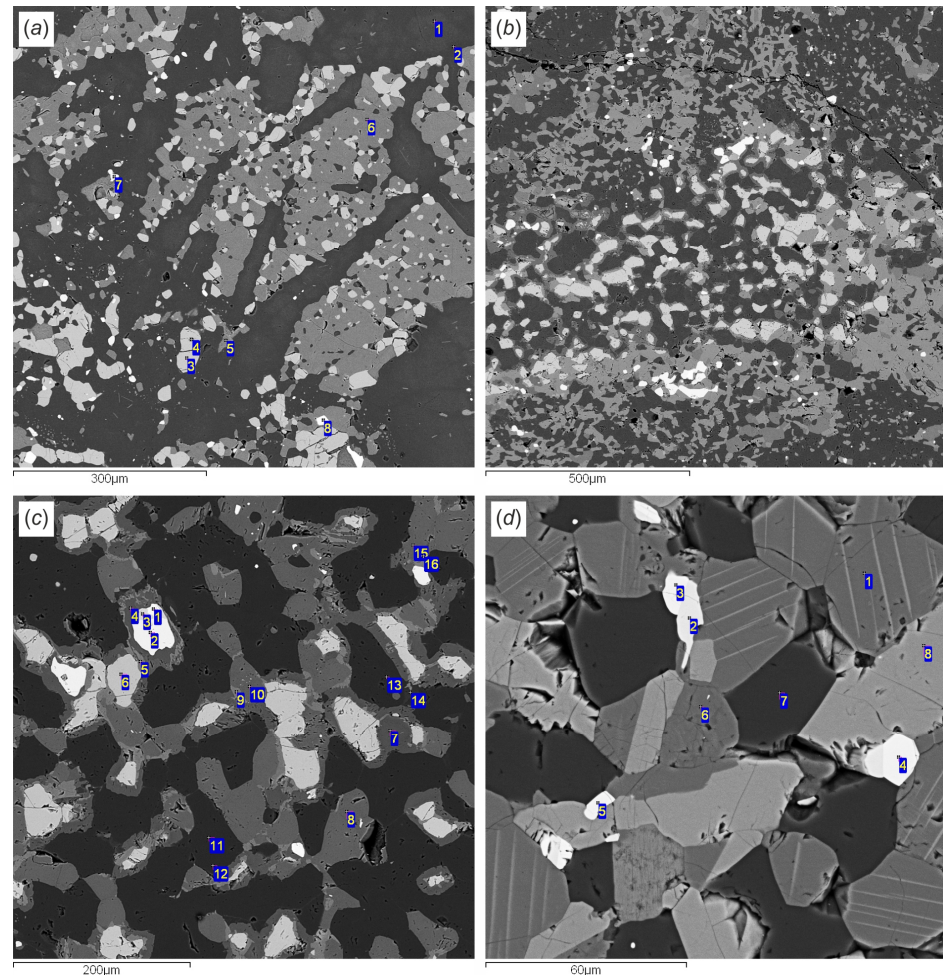

Figure 18. BSE images of beerbachite from Birkhin dikes. (**a**): beerbachite with remnant ophytic texture (sample SE01j2). Plagioclase laths with aggregates of olivine, orthopyroxene, clinopyroxene, and biotite among them. Ol(3)+Cpx(4,6)+Bt(5)+Ilm(7)+Pl(1,2). (**b**): mottled beerbachite (sample SE1843a). Mainly olivine with plagioclase in the center; two pyroxenes and amphibole with plagioclase at the bottom; biotite with plagioclase at the top. (**c**): granular beerbachite (sample SE1841a). Olivine grains in amphibole and orthopyroxene coats. Ol(6)+Opx(5,9,16)+Cpx(10,15)+Amp(7)+Bt(4)+Pl(11,12,13,14)+Cr-Spl(3)+Ilm(2)+Mag(1). (**d**): equigranular beerbachite (sample SE01j1). Orthopyroxene lamelli in clinopyroxene. Opx(8)+Cpx(1,6)+Pl(7)+Ilm(2)+Cr-Mag(3,4,5).

Amphibole is found either as individual, irregularly shaped grains or as rims over olivine or ilmenite. The compositions vary from magnesian hornblende to pargasite (10.4 to 16.0 wt.% Al_2O_3); TiO_2 is from 0.0 to 4.4 wt.% in different samples (Supplementary Table S4). The TiO_2 and #Mg values may vary even within a sample from 0.0 to 4.4 wt.% and 0.18 to 0.44, respectively, but Mg# ranges (0.62–0.75) are similar to those in the Shirokaya and Tazheran beerbachites in most of the samples.

Phlogopite is present in minor amounts in some beerbachite varieties. It has different forms: fine reddish-brown flakes; large irregularly shaped flat grains; rims over enclosed ilmenite; and symplectite with orthopyroxene. #Mg ranges from 0.43 to 0.84 (Supplementary Table S5); TiO2 is often high (5.4–6.7 wt.%) but is lower (3.1–3.5 wt.%) in some samples.

Plagioclase most often has andesine or labradorite compositions (X_{An} = 0.47–0.67), but is bytownitic (X_{An} = 0.73–0.90) in some samples (Supplementary Table S7). The grains are almost never zoned.

Cr spinel occurs infrequently and is present as individual fine grains or, less often, is intergrown with ilmenite (TiO_2 is as high as 14.2% in this case), and more rarely is symplectitic with orthopyroxene. The Birkhin Cr spinel differs from that in other beerbachite occurrences in low Al_2O_3 (4.8–29.4 wt.%) and #Mg (0.0–0.22) (Supplementary Table S6).

Ilmenite is present in modest amounts in all sampled rocks and has low #Mg (0.02–0.10) and variable but generally low manganese, at 0.37–1.95 wt.% TiO2 (Supplementary Table S8).

5.2. Conditions of Metamorphism

Estimating the *P-T* conditions of beerbachite metamorphism from data on mineral assemblages and mineral chemistry is challenging for several reasons. First of all, magmatic and high-temperature metamorphic assemblages are almost identical and hard to discriminate. Furthermore, the compositions of minerals failed to recover equilibrium during metamorphism, judging by large ranges of elements (e.g., in orthopyroxene) as well as the abundance of symplectites, which is a distinctive feature of the Olkhon beerbachites. Symplectites are vermicular intergrowths of two or more simultaneously growing minerals [43]. They may arise in different ways: exsolution, eutectic crystallization of residual melts (granophyres), metasomatism, solid-phase metamorphic reactions, etc. The best documented symplectites are vermicular myrmekites (quartz–high-silica plagioclase), widespread in granitoids and gneisses. Symplectites of other compositions are found in metamorphic, or less often, igneous and metasomatic rocks. The origin of symplectites is mostly associated with abrupt pressure and temperature changes, especially pressure, or with the effect of fluids at slow diffusion [43].

Symplectites in the analyzed beerbachite samples have diverse spinel–orthopyroxene, spinel–clinopyroxene, spinel–amphibole, phlogopite–orthopyroxene, or ilmenite–orthopyroxene compositions (Figures 12, 14 and 15). Eutectic crystallization of residual melts can hardly be responsible for this diversity, whereas solid-phase metamorphic reactions at low diffusion rates appear to be a more plausible mechanism. In this case, incomplete re-equilibration of minerals under changing *P-T* conditions is expected.

The systematic mineral chemistry changes observed in olivine, orthopyroxene, amphibole, plagioclase, and spinel indicate the presence of both magmatic and metamorphic phases in the samples. Given the obtained pressure estimates for metamorphism (see below) and the composition of high-temperature critical assemblages (Opx+Cpx+Ol), this metamorphic stage must correspond to the facies of pyroxene hornfels (beerbachite).

The variations in structural alteration degree from strong to absent in even proximal samples indicate that high-temperature metamorphism was apparently synchronous with the crystallization of mafic melts at a temperature approaching their solidus and thus required no additional heat source. On the other hand, the coexistence of brown Ti-hornblende and relatively low-temperature green actinolite/tremolite, cummigtonite, and interstitial carbonate in the same thin sections, as well as the absence of veinlets that would be produced by external inputs of CO_2-bearing fluids, suggest autometamorphic postmagmatic alteration.

Autometamorphism appears possible, judging by some structure and texture features:

- euhedral magmatic pyroxenes with anhedral (often poikilitic) metamorphic rims formed at a temperature about the solidus of gabbronorite and granulite facies, as the two-pyroxene assemblages have been recrystallized;
- inclusions of amphibole in olivine (Figure 15a), indicating that it crystallized before and was captured by olivine, against Bowen's series;
- significant discrete variations in mineral chemistry. The composition of amphibole may be homogeneous in some samples (e.g., in SE575a) or vary from magnesian hornblende to actinolite/tremolite and cummigtonite. In the same way, plagioclase can vary from bytownite to albite. Thus, only approximate bounds rather than precise estimates of

the temperature and pressure of metamorphism are obtainable in these conditions. We estimated the temperatures with two-pyroxene and amphibole geothermometers because our initial attempt at using the THERMOCALC 3.26 and AX2 thermodynamic algorithms [44] for the assemblage Ol+Cpx+Opx+Amp+Bt+Pl+Ilm+Spl had failed, apparently because the compositions of coexisting minerals were not equilibrated. The estimates obtained for several samples with different geothermometers [45–49] vary from 700 to 1100 °C, and the difference locally reached 100 °C even for different sites of a thin section. The amphibole–plagioclase geothermometer [50] yielded quite a narrow range (780–990 °C), and almost all temperatures exceeded 800 °C (granulite or pyroxene hornfels facies).

The pressure was estimated using Fershtater's [51] empirical amphibole–plagioclase geobarometer (Figure 19). The average values are generally low, mainly $\leq$ 2 kbar, and correspond to the hornfels facies of contact metamorphism. The pressure estimates for the Tazheran beerbachite are split into two groups: (i) ~2 kbar for the Shirokaya beerbachite and (ii) 4–5 kbar for samples with higher-silica plagioclase and more aluminous amphibole. The thermodynamic calculations with THERMOCALC 3.26 and AX2 [44] for the Tazheran assemblage Ol+Cpx+Opx+Amp+Bt+Pl+Ilm+Spl, at 700 to 900 °C, gave unrealistic high values (~7–9 kbar), also due to the lack of phase equilibrium, as in the case of temperature estimation.

To sum up, the peak temperature of metamorphism exceeded 800 °C at pressures within 2 kbar, or at depths of 6–7 km, while the Tazheran beerbachite may have undergone retrogressive metamorphism until low amphibolite facies and related gneissification.

5.3. Major- and Trace-Element Chemistry of the Olkhon Beerbachite

Here we provide a brief description of the geochemistry of the beerbachite. The detailed analysis of the geochemistry of the beerbachite is out of the scope of the paper, so we are planning to write a separate paper on the composition of the beerbachite where we will consider all these issues in detail. The analyzed beerbachite samples have mafic–ultramafic major-element compositions, with 42–50 wt.% SiO_2 (Figure 20, Supplementary Table S9), $\leq$ 3.5 wt.% alkalis, 6 to 26 wt.% MgO, and 7 to 17 wt.% Al_2O_3. The contents of MgO are in negative correlation with all major oxides, while other oxides (SiO_2-Al_2O_3-CaO-Na_2O-K_2O) are in positive correlation with one another. Therefore, the rock major-element chemistry depends mainly on relative percentages of olivine and plagioclase and lesser amounts of pyroxenes and oxide phases. The CaO/Al_2O_3 ratio ranges from 0.4 to 1.5 and shows no significant correlation with other components. The composition fields of the Tazheran and Shirokaya beerbachites generally overlap, though the samples of the latter are more magnesian while the former are more alkaline.

Most of the analyzed beerbachite samples have poorly fractionated REE spectra with (La/Yb)n = 1.8–4.5 (Figure 21; Supplementary Table S10). Two Tazheran samples, with relatively high REEs, show the highest TiO_2 enrichment (2.23–2.46 wt.%), while one sample has lower REE concentrations, a very low SiO_2 of 42.37, and an MgO of 18.21, quite high for beerbachite, due to high percentages of olivine. Two samples of the Shirokaya beerbachite, composed mainly of olivine, show low REE and (La/Yb)n = 0.7–0.9, MgO as high as 22.58–22.95 wt.%, and very low SiO_2 (43.06–43.77 wt.%). Most of the Shirokaya samples typically show a Nb minimum with $Nb_{PM}/\sqrt{(Th \times La)_{PM}}$ = 0.25–0.74 (Figure 21, Supplementary Table S10), which traces a suprasubduction component in the protolith. The $Nb_{PM}/\sqrt{(Th \times La)_{PM}}$ ratio in the Tazheran beerbachite is from 1.46 to 8.1, as it is typical of MORB and OIB, but the quite low $(Zr/Nd)_{PM}$ of 0.36–0.99 in all samples is uncommon to OIB.

5.4. Age of Olkhon Beerbachite

The beerbachite samples were dated by the U-Pb method on 43 zircon grains (45 LA-ICP-MS measurements). The analyzed zircons make up a single population according to grain morphology (Figure 22). They are mainly 80 to 200 μm (most often 100–150 μm) crystals or crystal fragments of short-prismatic habits with rounded edges and corners. In CL images, the zircons display sectorial or oscillatory zoning at moderate illumination. This sectorial

oscillatory zircon zonation is typical of igneous origin. They contain 84–564 ppm Th and 364–1462 ppm U, with a narrow Th/U range of 0.22–0.59. According to the dating results (Supplementary Table S11), all 45 measurements plot in one cluster around 472 ± 2 Ma, with a rms error of 4.0 (Figure 23).
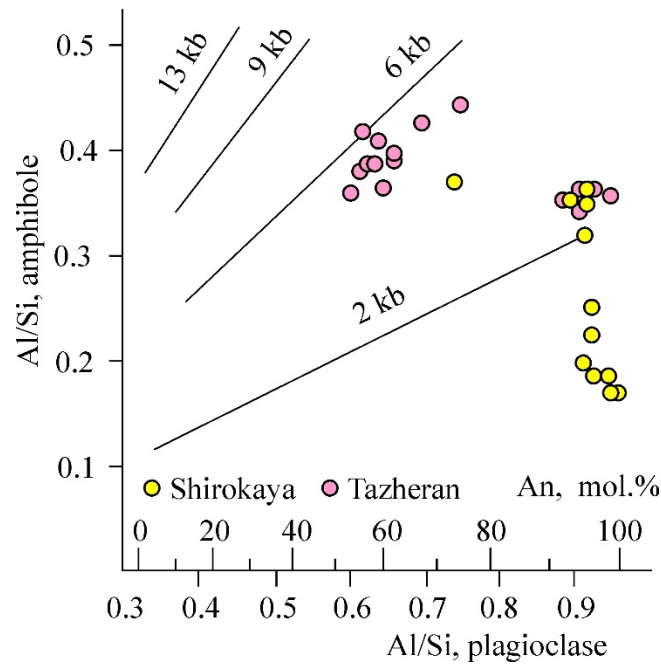

Figure 19. Amphibole–plagioclase geobarometer for high-Mg beerbachite of the Olkhon terrane, after Fershtater [51].
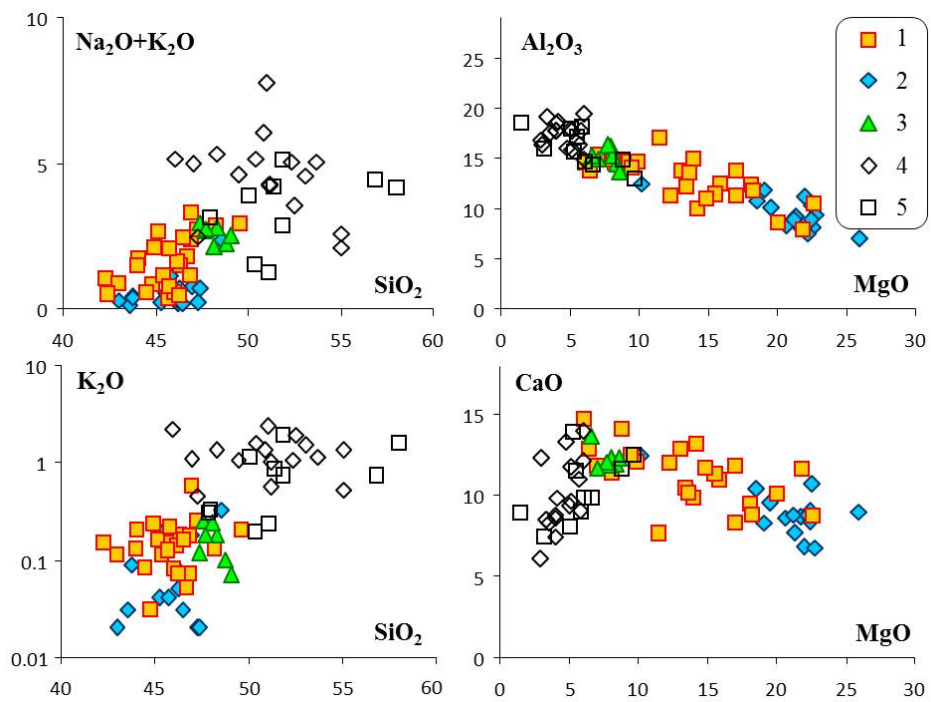

Figure 20. Tazheran (1), Shirokaya (2), and Birkhin (3) beerbachites in variaton diagrams. Amphibolite near the Tazheran (4) and Shirokaya (5) beerbachites. Element contents are in wt.%, Mg# = Mg/(Mg + Fe).
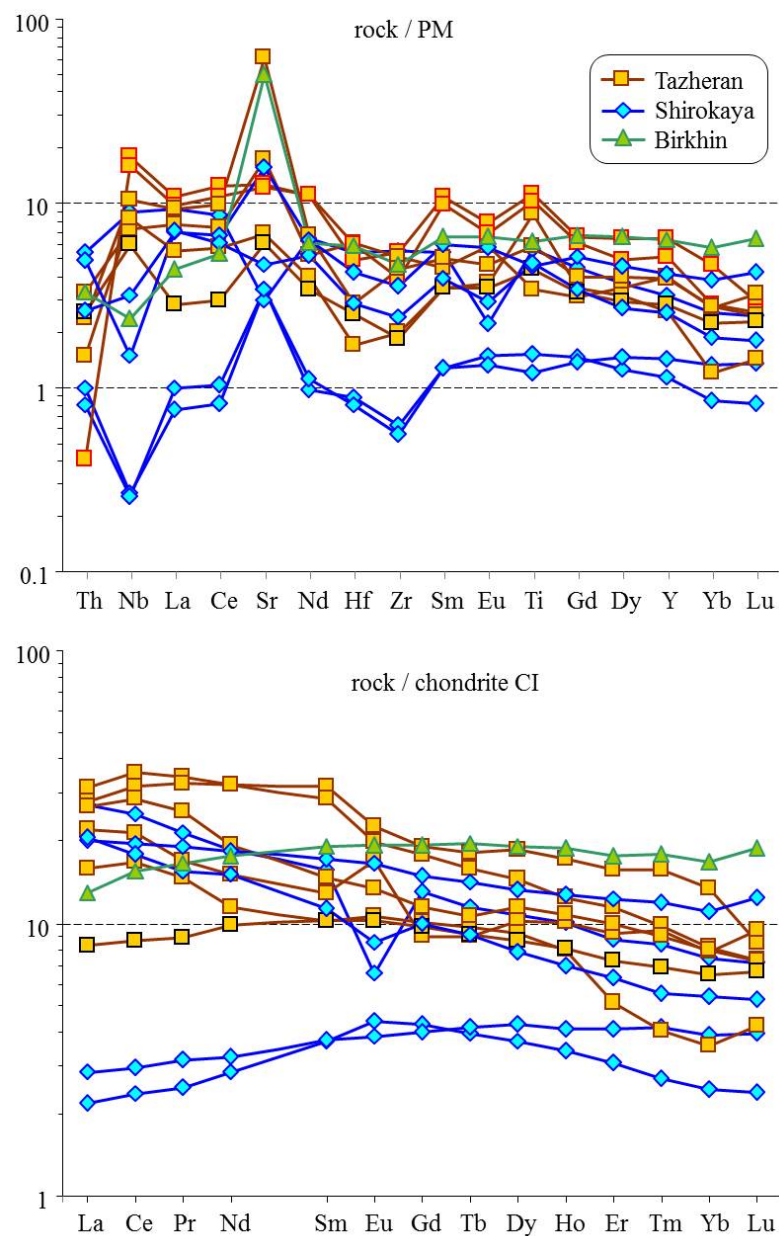
Figure 21. Spider diagram and REE patterns in Tazheran (1), Shirokaya (2), and Birkhin (3) beerbachites, normalized to PM according to [52].
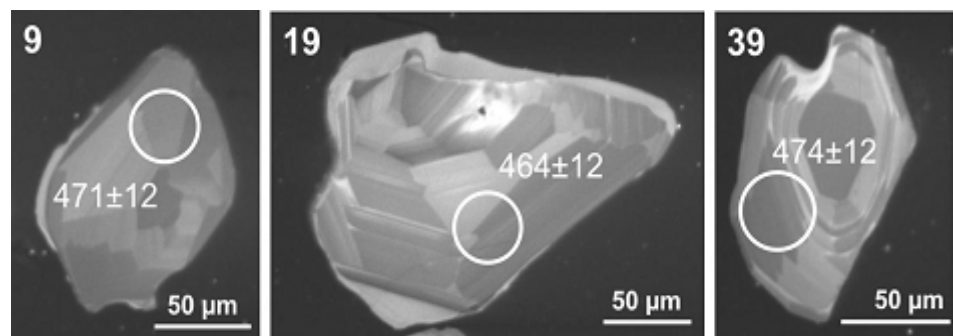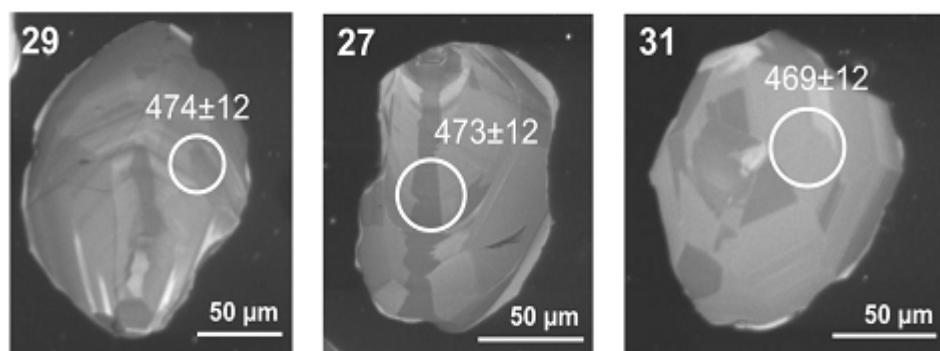

Figure 22. *Cont*.

Figure 22. Cathodoluminescence (CL) images of representative zircon crystals from Shirokaya beerbachite. Spot location and the respective ^{206}Pb/^{238}U ages are quoted with a 1-sigma error. Numbers in the top left corner correspond to numbers in Table S11 (Supplementary Materials).
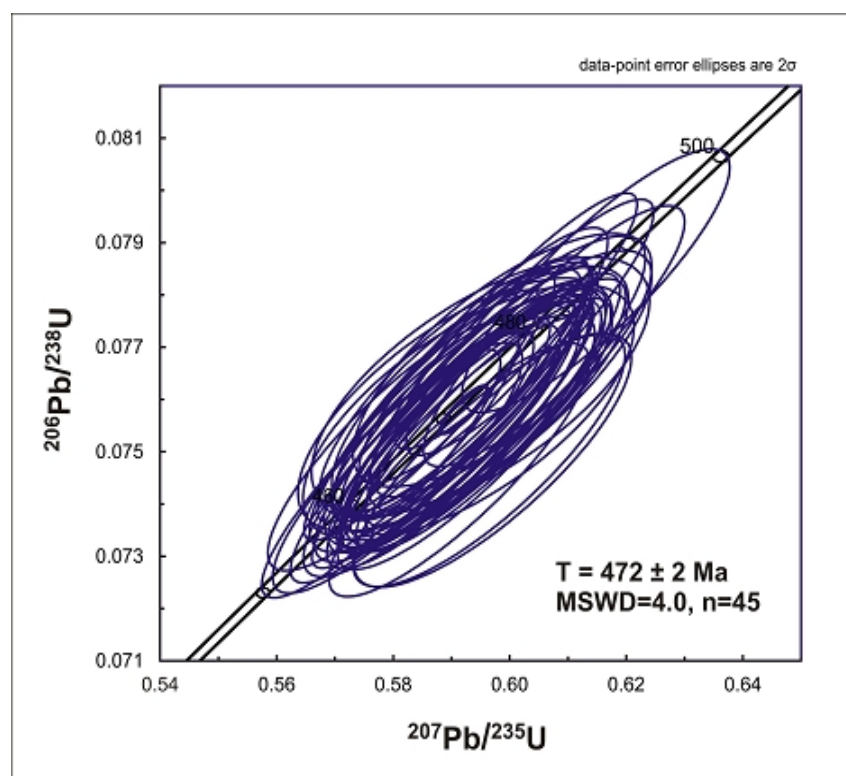

Figure 23. Concordia (Wetherill) diagram for ^{206}Pb/^{238}U ages of zircon from Shirokaya beerbachite. Error ellipses/bars are at the 2-sigma level. MSWD = mean squared weighted deviation.

6. Discussion

The mafic granular metamorphic rocks discovered in the Olkhon terrane could be identified as classical high-temperature hornfels in accordance with their mineralogy and petrography, but this interpretation contradicts other important factors, including the geological position of the rocks and the absence of potential heat sources in their vicinity that are required to produce classical hornfels. Therefore, the rocks are referred to as *beerbachite* due to their similarity to rocks described in the publications of the first half of the last century. The beerbachite occurrences in the Krestovsky subterrane are of three main types: (i) a broad, long zone between two gabbro intrusions in the Shirokaya Valley; (ii) rocks retaining fresh dolerite fragments coexisting with syenite in the Tazheran Massif; and (iii) dismembered dikes of plagioclase porphyrite on the periphery of the Birkhin gabbro complex. The location between the Krestovsky and Bora Elga intrusions (Figure 4) would imply an origin associated with metamorphism of the host amphibolite during the

emplacement of gabbro [23]. This idea is however inconsistent with (i) the presence of low-grade amphibolite facies along the boundary of the beerbachite zone with both gabbro intrusions (Figure 4); (ii) the lack of metamorphic zoning in beerbachite, with metamorphic grade variations due to sporadic occurrences of retrogressive metamorphism; (iii) the major- and trace-element chemistry of beerbachite strongly different from that of the host amphibolite (volcanic component of the volcanoplutonic complex), with a Ta-Nb minimum absent from the beerbachite spectra; (iv) the age of metamorphism about 30 Myr younger than the Birkhin complex: 472 Ma against 500 Ma [18]. The age difference is critical in this respect because, in our opinion, a period of 30 Myr is enough for gabbro to become colder than the temperature of beerbachite metamorphism. The 460–470 Ma Ust'-Krestovsky gabbro, roughly coeval to beerbachite, might be another candidate for an intrusive heat source, but it is located more than 1 km away and is separated from the beerbachite body by low-grade metamorphic rocks. Neither can the formation of beerbachite be due to high-temperature regional metamorphism, as the metamorphic grade of rocks in the Ust'-Krestovsky subterrane does not exceed the amphibolite facies limited to 500–600 °C. One more possible explanation would invoke the existence of a separate tectonic block in the area, but this hypothesis has no geological evidence.

The hornfels nature of the Tazheran beerbachite would appear more realistic, as the coexisting syenite intrusions might have provided the thermal alteration of the mafic rocks. That mechanism was suggested in the model by Konev and Samoilov in 1974 [53], implying the effect of syenite on the framework amphibolite. More so, this idea is in line with the age proximity of syenite and beerbachite and with the presence of dolerite, which preserved its magmatic structure despite the high-temperature effects. However, the contact metamorphic origin of the beerbachite is doubtful because Tazheran is not a simple in situ intrusive body in amphibolite but rather a tectonic feature bounded by blastomylonite sutures. Meanwhile, the beerbachite field occurs within the Tazheran Massif rather than in its surroundings and lacks metamorphic zoning where the grade would increase toward the contact syenite. The observed variations in metamorphic grade are more likely due to retrogressive metamorphism with the related syntectonic gneissification and formation of lower-temperature mineral assemblages (e.g., beerbachite at syenite contacts contains amphibole but lacks pyroxenes). Furthermore, amphibolite, unlike beerbachite, occurs as sills in a complex rock association with predominant marble and has a homogeneous mineralogy free from high-Mg varieties (Figure 21, Supplementary Table S9), which is another argument against the idea of syenite being a heat source for the beerbachite metamorphism.

The zone of dismembered beerbachite dikes on the margin of the Birkhin complex is traceable over 1 km and has no more than 15 m of visible thickness. The local geology, composition, and alteration sequence were discussed in a separate publication [16], and here we only note that different dike fragments underwent high-temperature metamorphism of different grades, from almost fresh porphyrite, by rocks with fully recrystallized pyroxenes but a preserved plagioclase framework, to granular beerbachite. This setting would appear to fit the model by Phillips [7], which attributes the unusual structure of dike rocks to the thermal effect of the still-hot, though already solid, injected gabbro. However, some features of the Birkhin complex and the position of the beerbachite dikes rather indicate that porphyrite and carbonate rocks intruded later, during 470–460 Ma strike–slip faulting [13]. The dike zone is only a fragment of an arc-shaped zone that traverses the whole gabbro body and is traceable by carbonate and skarn exposures.

Thus, for the time being, the autometamorphic mechanism of alteration under internal heat from the cooling melt appears to be the only plausible explanation for the paradoxical origin of beerbachite, with high-temperature metamorphism in the absence of an evident heat source. Correspondingly, we suggest reserving the name beerbachite, which is currently considered redundant, for hornfels-like rocks with the respective mineral assemblages produced by autometamorphism.

The formation setting of beerbachite is another problematic issue. It remains unclear why mafic magma most often crystallizes at shallow depths with the formation of typical ophytic, porphyritic, and other magmatic textures but occasionally undergoes complete recrystallization to form granular metamorphic rocks. The question has no appropriate answer yet, though a cautious conjecture may be made on the special role of some factors potentially favorable for recrystallization. First, the magnesian chemistry of dolerite (14–21 wt.% MgO) implies high temperatures of the melt and, hence, a high heat capacity of the igneous bodies. Second, magma was intruding in a period of active tectonic and metamorphic processes [13]. The tectonic history of the Olkhon terrane is composed of large-scale strike–slip faulting that culminated in the 470–460 Ma and was responsible for the linear geometry of most of the geological structures, except for relatively large rigid blocks (Birkhin and other gabbro bodies) subjected to rolling. Those movements may have produced particular shear zones in which fragments of geological bodies slid past one another, as in the case of the Birkhin gabbro [19]. The emplacement of mafic and ultramafic high-temperature melts in the shear zones and their syntectonic crystallization may have triggered the high-temperature auto-recrystallization of rocks. Furthermore, the relatively high temperatures of rocks (500–600 °C) intruded by the dike material likewise may be a cause of dolerite recrystallization.

7. Conclusions

The Olkhon collisional orogen accommodates beerbachite, a fine-grained granular mafic rock with a mineral assemblage of Opx+Cpx+Amp+Pl+Ilm±Ol±Bt±Spl±Ti-Mag and abundant symplectites, most often spinel-orthopyroxene, which we identify as beerbachite.

The Olkhon beerbachite occurrences are of three types. In the Shirokaya Valley, the 500 m × 1000 m beerbachite field lies between two 500 Ma gabbro intrusions of the Birkhin complex, and some beerbachite fragments are found in the adjacent marble melange. The 472 Ma age of beerbachite, ~30 Ma younger than gabbro, rules out the possibility for the latter to have been the heat source for metamorphism. Another occurrence of beerbachite is located within the Tazheran complex of igneous and metamorphic rocks: beerbachite, syenite, including nepheline syenite, subalkaline gabbro, and injection marbles. Finally, a dismembered beerbachite dike in the southern periphery of the 500 Ma Birkhin gabbro displays a complete sequence of dolerite alteration through typical granular beerbachite. The dike coexists with injection marbles and is a part of a large arc-shaped shear zone that traverses the gabbro body and may be associated with the rotation of a rigid block during the peak of strike–slip faulting activity (470–460 Ma).

The mineralogy and petrography of these rocks correspond to high-temperature hornfels (pyroxene–hornfels metamorphic facies), but the geological position and formation mechanism are different. We distinguish beerbachite as a separate rock type and argue in favor of this term, which has fallen into disuse. In this, we proceed from the absence of a heat source (intrusions that crystallized at temperatures above 800 °C) required for the high-temperature metamorphism in the immediate vicinity of the beerbachite bodies. The Olkhon beerbachite may have derived from dolerite and gabbro grading from ophytic to granular textures, which are locally preserved in the beerbachite occurrences. The alteration was apparently driven by autometamorphism, which apparently had a tectonic trigger and was maintained by the internal heat of the protolith under strike–slip deformation of the country rocks in shear zones where some parts of geological bodies slid past others. The emplacement of mafic magma during the peak of tectonic activity may have provided rapid recrystallization of magmatic minerals and the formation of the metamorphic rock structure.

beerbachite; Table S6: Selected analyses of spinel group minerals from the Olkhon beerbachite; Table S7: Selected analyses of plagioclases from the Olkhon beerbachite; Table S8: Selected analyses of ilmenite from the Olkhon beerbachite; Table S9: Major-element contents (wt.%) in the Olkhon beerbachite; Table S10: Trace-element contents (ppm) in the Olkhon beerbachite; Table S11: LA–SF-ICP–MS U–Pb dating data of zircon from beerbachite of the Olkhon terrane.

References

1. Warr, L.N. IMA–CNMNC approved mineral symbols. *Mineral. Mag.* **2021**, *85*, 291–320. [CrossRef]
2. Chelius, C. Das Granirmassive des Melibocus und siene Ganggestein. *Notizbl. Ver. Erdkd. Darmstadt Ser. 4* **1892**, *13*, 1–13.
3. Rosenbucsh, H. Analysis of beerbachite, Frankenstein, Odenwald. In *Element der Gesteinslehre*; E. Schweizerbart'sche Verlagshandlung: Stuttgart, Germany, 1901; 228p.
4. Klemm, G. Petrographische Mitteilungen aus dem Odenwalde. *Notizbl. Hessischen Landesamtes Bodenforsch. Wiesb.* **1926**, *9*, 104–117.
5. MacGregor, A.G. Scottish pyroxene-granulite hornfels and Odenwalde beerbachite. *Geol. Mag.* **1931**, *98*, 506–521. [CrossRef]
6. Bloxam, T.W. The origin of the Girvan–Ballantrae beerbachites. *Geol. Mag.* **1955**, *92*, 329–337. [CrossRef]
7. Phillips, E.R. On the rock name beerbachite. *Geol. Mag.* **1969**, *106*, 281–283. [CrossRef]
8. Dixey, F. The norite of Sierra Leone. *Quart. J. Geol. Soc. Lond.* **1922**, *78*, 299–343. [CrossRef]
9. Dixey, F. *The East African Rift System*; Colonial Geology and Mineral Resources Supplement Series; Bulletin Supplement no. 1; Her Majesty Stationery Office: London, UK, 1956; p. 115.
10. Wells, M.K. Sedimentary inclusions in the hypersthene-gabbro, Ardnamurchan, Argillshire. *Miner. Mag.* **1951**, *29*, 715–736.
11. Umeji, A.C. On the beerbachites from Freetown, Sierra Leone. *Geol. Mag.* **1985**, *122*, 663–667. [CrossRef]
12. Python, M.; Abily, B.; France, L. Magmatism and metamorphism at the sheeted dyke-gabbro transition zone: New insight from beerbachite from ODP/IODP Hole 1256D and Oman ophiolite. In *Geophysical Research Abstracts*; European Geosciences Union: Munich, Germany, 2014; Volume 16, EGU2014-14291.
13. Fedorovsky, V.S.; Sklyarov, E.V. The Olkhon geodynamic proving ground (Lake Baikal): High resolution satellite data and geological maps of new generation. *Geodyn. Tectonophys.* **2010**, *1*, 331–418. (In Russian) [CrossRef]
14. Donskaya, T.V.; Gladkochub, D.P.; Fedorovsky, V.S.; Sklyarov, E.V.; Cho, M.; Sergeev, S.A.; Demonterova, E.I.; Mazukabzov, A.M.; Lepekhina, E.N.; Cheong, W.; et al. Pre-Collisional (>0.5 Ga) Complexes of the Olkhon Terrane (Southern Siberia) as an echo of events in the Central Asian Orogenic Belt. *Gondwana Res.* **2017**, *42*, 243–263. [CrossRef]
15. Sklyarov, E.V.; Lavrenchuk, A.V.; Fedorovsky, V.S.; Gladkochub, D.P.; Donskaya, T.V.; Kotov, A.B.; Mazukabzov, A.M.; Starikova, A.E. Regional, contact metamorphism, and autometamorphism of the Olkhon Terrane (West Baikal Area). *Petrology* **2020**, *28*, 47–61. [CrossRef]
16. Gladkochub, D.P.; Donskaya, T.V.; Wingate, M.T.D.; Poller, U.; Kroner, A.; Fedorovsky, V.S.; Mazukabzov, A.M.; Todt, W.; Pisarevsky, S.A. Petrology, geochronology, and tectonic implications of c. 500 Ma metamorphic and igneous rocks along the northern margin of the Central-Asian Orogen (Olkhon terrane, Lake Baikal, Siberia). *J. Geol. Soc.* **2008**, *165*, 235–246. [CrossRef]
17. Volkova, N.I.; Vladimirov, A.G.; Travin, A.V.; Mekhonoshin, A.S.; Khromykh, S.V.; Yudin, D.S.; Rudnev, S.Y. U–Pb Isotopic dating of zircons (SHRIMP-II) from granulites of the Ol'khon Region of Western Baikal Area. *Dokl. Earth Sci.* **2010**, *432*, 821–824. [CrossRef]

18. Lavrenchuk, A.V.; Sklyarov, E.V.; Izokh, A.E.; Kotov, A.B.; Sal'nikova, E.B.; Fedorovsky, V.S.; Mazukabzov, A.M. Compositions of gabbro intrusions in the Krestovsky Zone (Western Baikal Region): A Record of plume–suprasubduction mantle interaction. *Russ. Geol. Geophys.* **2017**, *58*, 1139–1153. [CrossRef]

19. Fedorovsky, V.S.; Sklyarov, E.V.; Gladkochub, D.P.; Mazukabzov, A.M.; Donskaya, T.V.; Lavrenchuk, A.V.; Starikova, A.E.; Dobretsov, N.L.; Kotov, A.B.; Tevelev, A.V. *Aerospace Geological Map of the Olkhon Region (Baikal, Russia)*; Copymaster Center: Moscow, Russia, 2017.

20. Mekhonoshin, A.S.; Kolotilina, T.B.; Bukharov, A.A.; Goreglyad, A.V. Mafic plutonic complexes of the Olkhon area (Western Baikal region). In *Petrology of Igneous and Metamorphic Rocks*; University Press: Tomsk, Russia, 2001; pp. 165–170. (In Russian)

21. Pushkarev, E.V.; Lavrenchuk, A.V.; Gottman, I.A.; Sklyarov, E.V. Calcium ultramafites, ankaramite, and clinopyroxene-porphyric gabbro of the Birkhin Massif in the Ol'khon region: Solution of the problem of primary melt and formation. *Russ. Geol. Geophys.* **2023**, *64*, 1065–1085. [CrossRef]

22. Sklyarov, E.V.; Fedorovsky, V.S.; Kotov, A.B.; Lavrenchuk, A.V.; Mazukabzov, A.M.; Levitsky, V.I.; Sal'nikova, E.B.; Starikova, A.E. Carbonatites in collisional settings and pseudocarbonatites of the Early Paleozoic Ol'khon Collisional System. *Russ. Geol. Geophys.* **2009**, *50*, 1091–1106. [CrossRef]

23. Savel'eva, V.B.; Medvedeva, T.I. Mineralogy and conditions of formation of two-pyroxene and garnet—Hypersthene hornfels of the Anga Group of Western Baikal area. *Zapiski Rossiiskogo Mineralogicheskogo Obschestva* **1996**, *2*, 10–23.

24. Savelieva, V.B.; Uschapovskaya, Z.F.; Nartova, N.V. Kilchoanite rocks in the Olkhon region (West Baikal Region). *Zapiski Rossiiskogo Mineralogicheskogo Obschestva* **1992**, *12*, 111–117.

25. Galuskin, E.V.; Gfeller, F.; Savelyeva, V.B.; Armbruster, T.; Lazic, B.; Galuskina, I.O.; Többens, D.M.; Zadov, A.E.; Dzierżanowski, P.; Pertsev, N.N.; et al. Pavlovskyite $Ca_8(SiO_4)_2(Si_3O_{10})$: A new mineral of altered silicate-carbonate xenoliths from the two Russian type localities, Birkhin Massif, Baikal Lake area and Upper Chegem caldera, North Caucasus. *Am. Miner.* **2012**, *97*, 503–512. [CrossRef]

26. Sklyarov, E.V.; Fedorovsky, V.S.; Kotov, A.B.; Lavrenchuk, A.V.; Mazukabzov, A.M.; Starikova, A.E. Carbonate and silicate-carbonate injection complexes in collision systems: The West Baikal region as an example. *Geotectonics* **2013**, *47*, 180–196. [CrossRef]

27. Pashkova, G.V.; Panteeva, S.V.; Ukhova, N.N.; Chubarov, V.M.; Finkelshtein, A.L.; Ivanov, A.V.; Asavin, A.M. Major and trace elements in meimechites—Rarely occurring volcanic rocks: Developing optimal analytical strategy. *Geochem. Explor. Environ. Anal.* **2019**, *19*, 233–243. [CrossRef]

28. Panteeva, S.V.; Gladkochoub, D.P.; Donskaya, T.V.; Markova, V.V.; Sandimirova, G.P. Determination of 24 trace elements in felsic rocks by inductively coupled plasma mass spectrometry after lithium metaborate fusion. *Spectrochim. Acta* **2003**, *58*, 341–350. [CrossRef]

29. Griffin, W.L.; Powell, W.J.; Pearson, N.J.; O'Reilly, S.Y. GLITTER: Data reduction software for laser ablation ICP-MS, in Sylvester, P. In *Laser Ablation ICP-MS in the Earth Sciences: Current Practices and Outstanding Issues*; Short Course Series; Mineralogical Association of Canada: Québec City, QC, USA, 2008; Volume 40, pp. 307–311.

30. Hiess, J.; Condon, D.J.; McLean, N.; Noble, S.R. $^{238}U/^{235}U$ systematics in terrestrial uranium-bearing minerals. *Science* **2008**, *335*, 1610–1614. [CrossRef]

31. Slama, J.; Kosler, J.; Condon, D.J.; Crowley, J.L.; Gerdes, A.; Hanchar, J.M.; Horstwood, M.S.A.; Morris, G.A.; Nasdala, L.; Norberg, N.; et al. Plesovice zircon—A new natural reference material for U-Pb and Hf isotopic microanalysis. *Chem. Geol.* **2008**, *249*, 1–35. [CrossRef]

32. Jackson, S.E.; Pearson, N.J.; Griffin, W.L.; Belousova, E.A. The application of laser ablation-inductively coupled plasma-mass spectrometry to in situ U–Pb zircon geochronology. *Chem. Geol.* **2004**, *211*, 47–69. [CrossRef]

33. Ludwig, K. *User's Manual for Isoplot 3.00. A Geochronological Toolkit for Microsoft Excel*; Berkeley Geochronology Center: Berkeley, CA, USA, 2003; Volume 4, pp. 1–70.

34. Steiger, R.H.; Jäger, E. Subcommission on geochronology: Convention on the use of decay constants in geo- and cosmochronology. *Earth Planet. Sci. Lett.* **1977**, *36*, 359–362. [CrossRef]

35. Lindsley, D.H. Pyroxene thermometry. *Am. Miner.* **1983**, *68*, 477–493.

36. Dick, H.J.N.; Bullen, T. Chromian spinel as a petrogenetic indicator in abyssal and alpine-type peridotites and spatially associated lavas. *Contrib. Mineral. Petrol.* **1984**, *86*, 54–76. [CrossRef]

37. Barnes, S.J.; Roeder, P.L. The range of spinel compositions in terrestrial mafic and ultramafic rocks. *J. Petrol.* **2001**, *42*, 2279–2302. [CrossRef]

38. Ishii, T.; Robinson, P.T.; Maekawa, H.; Fiske, M. Petrological studies from diapiric serpentine seamounts in the Izu–Ogazawara–Mariana forearc. In *Proceeding of Ocean Drilling Program: Scientific Results*; Fryer, P., Pearce, J.A., Stokking, L.B., Eds.; (Ocean Drilling Program); Texas A & M University: College Station, TX, USA, 1992; Volume 125, pp. 445–485. [CrossRef]

39. Ohara, Y.; Ishii, T. Peridotites from the southern Mariana forearc: Heterogeneous fluid supply in the mantle wedge. *Isl. Arc* **1998**, *7*, 541–558. [CrossRef]

40. Evans, B.W.; Frost, B.R. Chrome-spine1 in progressive metamorphism: A preliminary analysis. *Geochim. Cosmochim. Acta* **1975**, *39*, 959–972. [CrossRef]

41. Loferski, P.J.; Lipin, B.R. Exsolution in metamorphosed chromite from the Red Lodge district, Montana. *Am. Miner.* **1983**, *68*, 777–789.

42. Van der Veen, H.; Maaskant, P. Chromian spinel mineralogy of the Stare Ransko gabbro-peridotite, Czech Republic, and its implications for sulfide mineralization. *Miner. Depos.* **1995**, *30*, 397–407. [CrossRef]
43. Vernon, R.H. *A Practical Guide to Rock Microstructure*; Cambridge University Press: Cambridge, UK, 2004; 594p.
44. Powell, R.; Holland, T.J.B. On thermobarometry. *J. Metamorph. Geol.* **2008**, *26*, 155–179. [CrossRef]
45. Brey, G.P.; Kohler, T. Geothermobarometry in four-phase lherzolites II, new thermobarometers, and practical assessment of existing thermobarometers. *J. Petrol.* **1990**, *31*, 1353–1378. [CrossRef]
46. Bertrand, P.; Mercier, J.-C.C. The mutual solubility of coexisting ortho- and clinopyroxene: Toward an absolute geothermometer for the natural system? *Earth Planet. Sci. Lett.* **1985**, *76*, 109–122. [CrossRef]
47. Blundy, J.D.; Holland, T.J.B. Calcic amphibole equilibria and a new amphibole-plagioclase geothermometer. *Contrib. Mineral. Petrol.* **1990**, *104*, 208–224. [CrossRef]
48. Wells, P.R.A. Pyroxene thermometry in simple and complex systems. *Contrib. Mineral. Petrol.* **1977**, *62*, 129–139. [CrossRef]
49. Wood, B.J.; Banno, S. Garnet-orthopyroxene and orthopyroxene-clinopyroxene relationships in simple and complex systems. *Contrib. Mineral. Petrol.* **1973**, *42*, 109–124. [CrossRef]
50. Fershtater, G.B. Empirical hornblende-plagioclase geobarometer. *Geokhimiya* **1990**, *3*, 328–335.
51. Holland, T.J.B.; Blundy, J.D. Non-ideal interactions in calcic amphiboles and their bearing on amphibole-plagioclase thermometry. *Contrib. Miner. Petrol.* **1994**, *116*, 433–447. [CrossRef]
52. Sun, S.S.; McDonough, W.F. Chemical and isotopic systematics of oceanic basalts: Implications for mantle composition and processes. In *Magmatism in Oceanic Basins*; Saunders, A.D., Norry, M.J., Eds.; Geological Society Special Publication: Cambridge, UK, 1989; Volume 42, pp. 313–346. [CrossRef]
53. Konev, A.A.; Samoilov, V.S. *Contact Metamorphism and Metasomatism in the Aureole of the Tazheran Alkaline Intrusion*; Nauka: Novosibirsk, Russia, 1974; p. 246. (In Russian)